

Exact solution for the Green’s function describing time-dependent thermal Comptonization

Peter A. Becker*

Center for Earth Observing and Space Research, George Mason University, Fairfax, VA 22030-4444, USA

Submitted 2002 December 26. Received ; in original form

ABSTRACT

We obtain an exact, closed-form expression for the time-dependent Green’s function solution to the Kompaneets equation. The result, which is expressed as the integral of a product of two Whittaker functions, describes the evolution in energy space of a photon distribution that is initially monoenergetic. Effects of spatial transport within a homogeneous scattering cloud are also included within the formalism. The Kompaneets equation that we solve includes both the recoil and energy diffusion terms, and therefore our solution for the Green’s function approaches the Wien spectrum at large times. This was not the case with earlier analytical solutions that neglected the recoil term and were therefore applicable only in the soft-photon limit. We show that the Green’s function can be used to generate all of the previously known steady-state and time-dependent solutions to the Kompaneets equation. The new solution allows the direct determination of the spectrum, without the need to numerically solve the partial differential equation. It is therefore much more convenient for data analysis purposes. Based upon the Green’s function, we derive a new, exact solution for the variation of the inverse-Compton temperature of an initially monoenergetic photon distribution. Furthermore, we also obtain a new time-dependent solution for the photon distribution resulting from the reprocessing of an optically thin bremsstrahlung initial spectrum with a low-energy cutoff. Unlike the previously known solution for bremsstrahlung injection, the new solution possesses a finite photon number density, and therefore it displays proper equilibration to a Wien spectrum at large times. The relevance of our results for the interpretation of emission from variable X-ray sources is discussed, with particular attention to the production of hard X-ray time lags, and the Compton broadening of narrow features such as iron lines.

Key words: radiation mechanisms: thermal — radiative transfer: line profiles — plasmas — galaxies: active — cosmology: early universe — methods: analytical — X-rays: general.

1 INTRODUCTION

In hot, radiation-dominated plasmas, the primary interaction between photons and electrons occurs via Compton scattering. This process consequently plays a central role in the formation of X-ray spectra in a variety of sources, including active galaxies, low-mass X-ray binaries, and the early universe. The repeated scattering of radiation off free electrons (Comptonization) can have a profound effect on both the X-ray spectrum and the Fourier structure of the observed emission in the time domain. The effect of multiple Compton scattering depends on the velocity distribution of the electrons; random and systematic motions of the electrons produce “thermal” and “bulk” Comptonization, respectively. Thermal Comptonization can explain the formation of the power-law tails observed in the X-ray spectra from active galaxies and low-mass X-ray binaries, as well as the development of time lags between the hard and soft photons (Shapiro, Lightman, & Eardley 1976; Sunyaev & Titarchuk 1980; van der Klis et al. 1987; Stollman et al. 1987). This process also governs the evolution of the cosmic background radiation

* E-mail: pbecker@gmu.edu

before recombination (Sunyaev & Zeldovich 1970; Zeldovich & Sunyaev 1969; Illarionov & Sunyaev 1975a, 1975b), and it is a necessary ingredient in models for the production of the modified blackbody continuum emission observed during X-ray bursts (Sunyaev & Titarchuk 1980; Titarchuk 1988). Thermal Comptonization also seems to contribute to the broadening of the $K\alpha$ iron lines observed in a number of sources (Reynolds & Wilms 2000; Wang, Zhou, & Wang 1999; Ross, Fabian, & Young 1999). In addition to the thermal process, bulk Comptonization can also influence the spectral formation when the electrons are converging on average, as for example in a radiation-dominated shock or a quasi-spherical accretion flow (Payne & Blandford 1981; Lyubarskii & Sunyaev 1982; Becker 1988; Colpi 1988; Titarchuk, Mastichiadis, & Kylafis 1997; Titarchuk & Zannias 1998; Laurent & Titarchuk 2001; Titarchuk & Shrader 2002).

The effect of thermal Comptonization on the photon distribution is described by the well-known Kompaneets partial differential equation, published in 1957. This equation, based on a Fokker-Planck formalism, describes the effect of multiple Compton scattering on the photon distribution when the electrons are moving nonrelativistically and the average fractional energy change per scattering is small. The Kompaneets equation has provided the foundation for most of the theoretical studies of thermal Comptonization in astrophysical environments, which have focused primarily on the steady-state reprocessing of monoenergetic radiation injected continuously into a nonrelativistic plasma with time-independent properties (e.g., Katz 1976; Sunyaev & Titarchuk 1980). These studies have provided useful insight into the formation of the ubiquitous power-law spectra observed in the quiescent emission from active galactic nuclei (AGNs) and galactic black-hole candidates. Titarchuk & Lyubarskij (1995) generalized these results by solved the stationary form of the Boltzmann kinetic equation to demonstrate that power-law spectra can also result from Comptonization in a cloud of relativistic electrons. Despite the success of the steady-state models in helping us to understand the formation of the quiescent X-ray spectra, they cannot be used to follow the spectral and temporal evolution of rapid transients. This is a concern because rapid variability is a characteristic feature of many classes of X-ray sources. Indeed, the rapid variability itself contains detailed information about the geometry and spatial structure of the inner region of the accretion flow. Analysis of the ‘‘Compton reverberations’’ associated with the impulsive injection of soft photons can provide perhaps the most direct probe of the inner region (Reynolds et al. 1999; Ulrich 2000). Specific examples of rapid variability include the strong X-ray flares observed from the Seyfert galaxies NGC 4151 (Tananbaum et al. 1978; Lawrence 1980) and NGC 6814 (König et al. 1997; Mittaz & Branduardi-Raymont 1989) in which the intensity increases by a factor of 5-10 in $\lesssim 1000$ s. Many other active galaxies also display significant variability (see, e.g., Iwasawa et al. 2000; Merloni & Fabian 2001), and flickering and bimodal spectral behavior on timescales of seconds involving substantial fractions of the X-ray flux have been observed from Cyg X-1 (Tanaka 1989; Zdziarski et al. 2002), GX 339-4 (Kitamoto 1989; Miyamoto et al. 1991), and other galactic black-hole candidates (Mereghetti 1993; Smith, Heindl, & Swank 2002).

Observations of rapid variability during strong X-ray transients in AGNs and galactic black-hole candidates suggest that a time-dependent model for the spectral formation may be required in order to understand the physical processes occurring in the source plasma. Surprisingly, the time-dependent Green’s function associated with the Kompaneets equation has never been obtained in closed form. Time-dependent analytical solutions previously discussed in the literature have focused on certain special cases, or have adopted simplifying approximations. For example, Chapline and Stevens (1973) examined the Comptonization of a bremsstrahlung initial spectrum in a plasma with steady properties. However, the time-dependent analytical solution they obtain is unphysical in the sense that full equilibration to a Wien spectrum never occurs because the initial spectrum contains an infinite number of low-energy photons. Zeldovich & Sunyaev (1969) and Payne (1980) derived the Green’s function for time-dependent thermal Comptonization under the assumption that $\epsilon \ll kT_e$, where T_e is the electron temperature and ϵ is the photon energy. Under this restriction, the effect of electron recoil can be ignored, and the transport equation admits a relatively simple solution for the Green’s function. However, this ‘‘soft-photon’’ Green’s function is not valid when photons remain in the plasma long enough to upscatter to energies comparable to the electron thermal energy, which cannot be ruled out in the observed transients. Further discussion of this point is provided in § 6.1.

More general results have been obtained using numerical simulations based on a modified form of the Kompaneets equation that includes an additional term describing spatial diffusion. For example, Böttcher & Liang (1998) simulated numerically the Compton upscattering of flares of soft radiation in clouds with various geometries, and Malzac & Jourdain (2000) utilized a Monte-Carlo code to model time-dependent Comptonizing flares in a corona with a self-consistently determined temperature. The utilization of partial differential equation solvers or Monte-Carlo simulations to analyze the transport equation is a complex procedure that is inconvenient from the point of view of X-ray data analysis. Furthermore, the results obtained for the spectra often depend on boundary conditions in the energy coordinate that are not known with precision a priori. In order to limit the effect of the imprecisely known boundary conditions on the computed spectrum, one is usually forced to extend the computational domain well beyond the region of interest. The associated decrease in computational efficiency reduces the utility of simulations based on numerical integration of the transport equation. Moreover, even when accurate numerical solutions can be obtained, it is often difficult to extract simple analytical estimates from them due to the complexity of the simulations.

Our increasing capability to make observations with high temporal and spectral resolution presents us with an interesting theoretical challenge, which is to obtain a closed-form expression for the X-ray spectrum resulting from the thermal Comptonization of initially monoenergetic photons in an ionized plasma. The availability of such a solution would be of great

importance for our understanding of spectral formation during rapid X-ray transients, and particularly when the Compton broadening of narrow features such as iron lines is of interest. As a first step, in this paper we analyze the transport equation for thermal Comptonization and derive the time-dependent Green's function for the case of a homogeneous plasma with steady properties. Our goal is to obtain the “complete” Green's function, including the effect of electron recoil as well as the diffusion of photons in the energy space. The formalism also incorporates a treatment of spatial transport inside the cloud. The resulting solution can be used to obtain a comprehensive understanding of the spectral evolution due to thermal Comptonization in a plasma with any shape and with any temporal and spatial distribution of embedded photon sources. We believe that the insights gained using this new solution will be valuable for the interpretation of current and future X-ray data from active galaxies and low-mass X-ray binaries.

The remainder of the paper is organized as follows. In § 2 we introduce and discuss the fundamental transport equation governing the propagation of photons in X-ray emitting plasma clouds. In § 3 the transport equation is solved to obtain the formal solution for the time-dependent Green's function in the energy domain as an integral of a product of two Whittaker functions. The properties of the Green's function are explored in § 4, where we also obtain a particular solution describing the evolution a bremsstrahlung initial spectrum including a low-energy cutoff. Specific examples of the time-dependent energy spectra emitted by Comptonizing clouds are computed in § 5, and the implications of our results for the interpretation of X-ray data are discussed in § 6. Supplemental technical details of the mathematical approach are provided in Appendix A.

2 TIME-DEPENDENT COMPTONIZATION

In radiation-dominated, fully-ionized plasmas, photon creation and destruction are unable to establish local thermodynamic equilibrium, and the photons and electrons interact primarily via Compton scattering. In this section, we discuss the general equations governing the photon distribution as a function of time, space, and energy. The evolution equation for the photon energy distribution is solved in § 3.

2.1 Transport equation

Neglecting absorption, the temporal evolution of the distribution of photons in a nonrelativistic plasma cloud with electron number density n_e and electron temperature T_e is governed by the transport equation (Katz 1976; Payne 1980)

$$\frac{\partial \bar{n}}{\partial t} = \frac{n_e \sigma_T c}{m_e c^2} \frac{1}{\epsilon^2} \frac{\partial}{\partial \epsilon} \left[\epsilon^4 \left(\bar{n} + \bar{n}^2 + kT_e \frac{\partial \bar{n}}{\partial \epsilon} \right) \right] + \vec{\nabla} \cdot \left(\frac{c}{3n_e \sigma_T} \vec{\nabla} \bar{n} \right) + j, \quad (1)$$

where $\bar{n}(\epsilon, \vec{r}, t)$ is the photon occupation number (a dimensionless quantity), ϵ is the photon energy, t is time, \vec{r} is the spatial location within the plasma, σ_T is the Thomson cross section, c is the speed of light, m_e is the electron mass, and k is Boltzmann's constant. The specific intensity, $I_\nu \propto \text{ergs cm}^{-2} \text{s}^{-1} \text{ster}^{-1} \text{Hz}^{-1}$, is related to the occupation number by $I_\nu = (2h\nu^3/c^2) \bar{n}$, where h is Planck's constant and $\nu = \epsilon/h$ is the photon frequency. The terms on the right-hand side of equation (1) represent thermal Comptonization, spatial diffusion, and photon sources, respectively. We shall assume that I_ν , \bar{n} , and the source term j are all isotropic. In this paper we will focus primarily on the process of thermal Comptonization occurring in homogeneous plasmas with steady properties. Effects related to bulk motion and temperature variations will be discussed in § 6.

The occupation number \bar{n} can be integrated with respect to ϵ to obtain the total radiation number density, given by

$$n_r(\vec{r}, t) = \int_0^\infty \frac{8\pi}{c^3 h^3} \epsilon^2 \bar{n}(\epsilon, \vec{r}, t) d\epsilon. \quad (2)$$

The \bar{n}^2 term in equation (1) describes stimulated scattering and is rarely important in astrophysical applications. When this term is neglected, the transport equation is rendered linear, and in the case of an isothermal plasma, we can obtain the equivalent form

$$\frac{\partial \bar{n}}{\partial t} = \frac{n_e \sigma_T c kT_e}{m_e c^2} \frac{1}{x^2} \frac{\partial}{\partial x} \left[x^4 \left(\bar{n} + \frac{\partial \bar{n}}{\partial x} \right) \right] + \vec{\nabla} \cdot \left(\frac{c}{3n_e \sigma_T} \vec{\nabla} \bar{n} \right) + j, \quad (3)$$

where we have introduced the dimensionless photon energy

$$x(\epsilon) \equiv \frac{\epsilon}{kT_e}. \quad (4)$$

By transforming the variable of integration in equation (2) from ϵ to x , we can reexpress the photon number density as

$$n_r(\vec{r}, t) = 8\pi \left(\frac{kT_e}{ch} \right)^3 \int_0^\infty x^2 \bar{n}(x, \vec{r}, t) dx. \quad (5)$$

Since equation (3) is linear in \bar{n} , it is sufficient to consider a source term $j = j_*$ that is localized in time, space, and energy, given by

$$j_* \equiv \frac{1}{8\pi x_0^2} \left(\frac{hc}{kT_e} \right)^3 \delta(t - t_0) \delta(\vec{r} - \vec{r}_0) \delta(x - x_0), \quad (6)$$

which represents the injection of a single photon with dimensionless energy $x_0 = \epsilon_0/(kT_e)$ at time t_0 and location \vec{r}_0 . The solution to equation (3) corresponding to the source term j_* is the Green's function, $\bar{n}_G(x, x_0, \vec{r}, \vec{r}_0, t, t_0)$, describing the process of time-dependent thermal Comptonization in an isothermal plasma.

Once the Green's function has been determined by solving equations (3) and (6) in combination with a suitable boundary condition imposed at the surface of the cloud, the response to a general source term j can be obtained by performing the convolution

$$\bar{n}(x, \vec{r}, t) = 8\pi \left(\frac{kT_e}{ch} \right)^3 \oint_V \int_0^t \int_0^\infty \bar{n}_G(x, x_0, \vec{r}, \vec{r}_0, t, t_0) j(x_0, t_0, \vec{r}_0) x_0^2 dx_0 dt_0 d^3 \vec{r}_0, \quad (7)$$

where the \vec{r}_0 integration proceeds over the entire volume V of the cloud, regardless of its shape. Equation (7) implicitly assumes that no radiation is present in the cloud at time $t = 0$, and that no radiation is incident on the cloud from the outside. As an alternative to solving for \bar{n}_G using equations (3) and (6), we point out that \bar{n}_G is also the solution to the *homogeneous* equation

$$\frac{\partial \bar{n}_G}{\partial t} = \frac{n_e \sigma_T c kT_e}{m_e c^2} \frac{1}{x^2} \frac{\partial}{\partial x} \left[x^4 \left(\bar{n}_G + \frac{\partial \bar{n}_G}{\partial x} \right) \right] + \vec{\nabla} \cdot \left(\frac{c}{3 n_e \sigma_T} \vec{\nabla} \bar{n}_G \right), \quad (8)$$

subject to the *initial condition*

$$\bar{n}_G(x, x_0, \vec{r}, \vec{r}_0, t, t_0) \Big|_{t=t_0} = \frac{1}{8\pi x_0^2} \left(\frac{hc}{kT_e} \right)^3 \delta(\vec{r} - \vec{r}_0) \delta(x - x_0). \quad (9)$$

The homogeneity of equation (8) makes it a more convenient starting point than equation (3) for the determination of the Green's function \bar{n}_G . In a homogeneous plasma with steady properties, both T_e and n_e are constants, and it is convenient to rewrite equation (8) as

$$\frac{\partial \bar{n}_G}{\partial y} = \frac{1}{x^2} \frac{\partial}{\partial x} \left[x^4 \left(\bar{n}_G + \frac{\partial \bar{n}_G}{\partial x} \right) \right] + \vec{\nabla} \cdot \left(\frac{c}{3 \alpha n_e \sigma_T} \vec{\nabla} \bar{n}_G \right), \quad (10)$$

where we have introduced the dimensionless time

$$y(t) \equiv \alpha (t - t_0), \quad \alpha \equiv n_e \sigma_T c \frac{kT_e}{m_e c^2}. \quad (11)$$

This is the familiar Compton y -parameter, which generally must exceed unity in order for significant modification of the spectrum to occur (Rybicki & Lightman 1979). The constant α is the ‘‘Comptonization rate,’’ and $y = 0$ at the initial time $t = t_0$. In the case of a homogeneous plasma with constant density and temperature, the temporal evolution of the photon distribution depends only on the elapsed time since injection, $t - t_0$, and therefore we can write $\bar{n}_G(x, x_0, \vec{r}, \vec{r}_0, t, t_0) = \bar{n}_G(x, x_0, \vec{r}, \vec{r}_0, y)$ without loss of generality.

By operating on equation (10) with $8\pi(kT_e/hc)^3 \int_0^\infty x^2 dx$, we can show that the radiation number density associated with the Green's function,

$$\eta(\vec{r}, \vec{r}_0, y) \equiv 8\pi \left(\frac{kT_e}{ch} \right)^3 \int_0^\infty x^2 \bar{n}_G(x, x_0, \vec{r}, \vec{r}_0, y) dx, \quad (12)$$

satisfies the homogeneous spatial diffusion equation

$$\frac{\partial \eta}{\partial y} = \vec{\nabla} \cdot \left(\frac{c}{3 \alpha n_e \sigma_T} \vec{\nabla} \eta \right). \quad (13)$$

Note that the Comptonization term in equation (10) vanishes upon integration, which is a manifestation of the fact that Compton scattering does not create or destroy photons. The initial condition for η can be obtained by combining equations (9) and (12), which yields

$$\eta(\vec{r}, \vec{r}_0, y) \Big|_{y=0} = \delta(\vec{r} - \vec{r}_0). \quad (14)$$

Note that equations (13) and (14) must be supplemented by a suitable flux boundary condition imposed at the surface of the cloud in order to account for the escape of radiation from the plasma.

2.2 Separability

We shall focus on the evolution of the occupation number Green's function \bar{n}_G subject to the initial condition given by equation (9). The transport equation (10) is separable in time, space, and energy when n_e and T_e are constants, as assumed here (Payne 1980). We employ separability by writing the occupation number \bar{n} as the product

$$\bar{n}_G(x, x_0, \vec{r}, \vec{r}_0, y) = \frac{1}{8\pi} \left(\frac{hc}{kT_e} \right)^3 \eta(\vec{r}, \vec{r}_0, y) f_G(x, x_0, y), \quad (15)$$

where $f_G(x, x_0, y)$ is the Green's function for the photon energy distribution. Note that the energy and spatial dependences have been separated since the former is contained in f_G and the latter is contained in η . Substituting for \bar{n}_G in the transport equation (10) using equation (15), and utilizing the fact that η satisfies equation (13), we can show that the energy distribution f_G satisfies the Kompaneets (1957) Fokker-Planck equation,

$$\frac{\partial f_G}{\partial y} = \frac{1}{x^2} \frac{\partial}{\partial x} \left[x^4 \left(f_G + \frac{\partial f_G}{\partial x} \right) \right], \quad (16)$$

along with the initial condition

$$f_G(x, x_0, y) \Big|_{y=0} = x_0^{-2} \delta(x - x_0). \quad (17)$$

The terms proportional to f_G and $\partial f_G / \partial x$ inside the parentheses on the right-hand side of equation (16) express the effects of electron recoil and stochastic (second-order Fermi) photon energization, respectively. Due to our neglect of stimulated scattering, the asymptotic solution to equation (16) obtained as $y \rightarrow \infty$ is the Wien spectrum $f_G \propto e^{-x}$, rather than a Bose-Einstein distribution. The function $f_G(x, x_0, y)$ represents the solution to the Kompaneets equation in an infinite, homogeneous medium. Spatial effects associated with the geometry and the finite size of the scattering cloud are introduced via the density distribution $\eta(\vec{r}, \vec{r}_0, y)$. Note that \bar{n}_G satisfies the initial condition given by equation (9) as required.

Once the spatial distribution has been obtained by solving equation (13) for $\eta(\vec{r}, \vec{r}_0, y)$, we must next determine the energy distribution $f_G(x, x_0, y)$ in order to construct the complete solution for \bar{n}_G using equation (15). Although Payne (1980) and Rybicki & Lightman (1979) state that equation (16) must be solved numerically in general, we shall demonstrate below that an analytical solution for the Green's function can in fact be obtained in the form of a real integral. By operating on equation (16) with $\int_0^\infty x^2 dx$, we can establish that f_G has the convenient normalization

$$\int_0^\infty x^2 f_G(x, x_0, y) dx = \text{constant} = 1, \quad (18)$$

where the final result follows from the initial condition (eq. [17]). Note that this normalization is maintained for all values of y , which reflects the fact that Compton scattering conserves photons. We shall seek to solve equation (16) using Laplace transformation in § 3. Once the solution for the Green's function $f_G(x, x_0, y)$ is known, the particular solution for the distribution function $f(x, y)$ corresponding to an arbitrary initial spectrum $f_0(x)$ can be found using the integral formula

$$f(x, y) = \int_0^\infty x_0^2 f_0(x_0) f_G(x, x_0, y) dx_0. \quad (19)$$

By operating on equation (19) with $\int_0^\infty x^2 dx$, we can establish that

$$I_2(y) \equiv \int_0^\infty x^2 \int_0^\infty x_0^2 f_0(x_0) f_G(x, x_0, y) dx_0 dx = \int_0^\infty x_0^2 f_0(x_0) dx_0 = \text{constant}, \quad (20)$$

where the final result is obtained by reversing the order of integration and applying equation (18). The constancy of I_2 follows from the fact that Comptonization does not create or destroy photons, and we therefore refer to I_2 as the ‘‘number moment’’ of the particular solution $f(x, y)$. Equation (20) will provide a useful check when we consider the properties of the particular solutions obtained in § 4.

3 SOLUTION FOR THE GREEN'S FUNCTION

Our analytical approach to the determination of the Green's function energy distribution $f_G(x, x_0, y)$ will be based on Laplace transformation. For the sake of brevity, only the primary steps are discussed here. Readers interested in the technical details are referred to Appendix A.

3.1 Laplace transformation

Laplace transformation of the Kompaneets partial differential equation (16) with respect to y yields the ordinary differential equation

$$sL - x_0^{-2} \delta(x - x_0) = \frac{1}{x^2} \frac{d}{dx} \left[x^4 \left(L + \frac{dL}{dx} \right) \right], \quad (21)$$

where

$$L(x, x_0, s) \equiv \int_0^\infty e^{-sy} f_G(x, x_0, y) dy \quad (22)$$

denotes the Laplace transform of $f_G(x, x_0, y)$, and we have also used equation (17). We show in Appendix A.1 that the solution for the transform $L(x, x_0, s)$ is given by

$$L(x, x_0, s) = \frac{\Gamma(\mu - 3/2)}{\Gamma(1 + 2\mu)} x_0^{-2} x^{-2} e^{(x_0 - x)/2} \begin{cases} W_{2, \mu}(x_0) M_{2, \mu}(x), & x \leq x_0, \\ M_{2, \mu}(x_0) W_{2, \mu}(x), & x \geq x_0, \end{cases} \quad (23)$$

where the quantity μ is a function of the transform variable s , defined by

$$\mu(s) \equiv \left(s + \frac{9}{4} \right)^{1/2}, \quad (24)$$

and $M_{2, \mu}(x)$ and $W_{2, \mu}(x)$ denote the Whittaker functions (Abramowitz & Stegun 1970). Equation (23) can be rewritten in the equivalent form

$$L(x, x_0, s) = \frac{\Gamma(\mu - 3/2)}{\Gamma(1 + 2\mu)} x_0^{-2} x^{-2} e^{(x_0 - x)/2} M_{2, \mu}(x_{\min}) W_{2, \mu}(x_{\max}), \quad (25)$$

where

$$x_{\min} \equiv \min(x, x_0), \quad x_{\max} \equiv \max(x, x_0). \quad (26)$$

The function $W_{2, \mu}(x)$ is defined in terms of $M_{2, \mu}(x)$ by equation (13.1.34) of Abramowitz & Stegun (1970), which gives

$$W_{2, \mu}(x) \equiv \frac{\Gamma(-2\mu)}{\Gamma(-\mu - 3/2)} M_{2, \mu}(x) + \frac{\Gamma(2\mu)}{\Gamma(\mu - 3/2)} M_{2, -\mu}(x), \quad (27)$$

and the function $M_{2, \mu}(x)$ can be evaluated using the series expansion

$$M_{2, \mu}(x) = e^{-x/2} x^{\mu+1/2} \left[1 + \frac{\mu - 3/2}{1 + 2\mu} x + \frac{(\mu - 3/2)(\mu - 1/2)}{(1 + 2\mu)(2 + 2\mu)} \frac{x^2}{2} + \dots \right]. \quad (28)$$

The solution for $L(x, x_0, s)$ in equation (25) has been obtained by utilizing continuity and derivative jump conditions based on the differential equation (21), along with various identities satisfied by the Whittaker functions. Further details of the derivation are provided in Appendix A.1.

3.2 Integral expression for the Green's function

To obtain the solution for the Green's function $f_G(x, x_0, y)$, we must perform the inverse Laplace transformation of $L(x, x_0, s)$ using the complex Mellin inversion integral (Butkov 1968),

$$f_G(x, x_0, y) = \frac{1}{2\pi i} \int_{\gamma - i\infty}^{\gamma + i\infty} e^{sy} L(x, x_0, s) ds, \quad (29)$$

where the constant γ is selected so that the line $\text{Re } s = \gamma$ lies to the right of any singularities in the integrand. In this problem, singularities occur where the quantity $\mu - 3/2$ is zero or a negative integer, resulting in the divergence of $\Gamma(\mu - 3/2)$. The definition of μ (eq. [24]) therefore implies that simple poles are located at $s = 0$ and $s = -2$. The corresponding values for μ are $\mu = 3/2$ and $\mu = 1/2$, respectively. From the locations of the singularities, it follows that we must require $\gamma > 0$ for convergence of the integral in equation (29).

The simple poles at $s = 0$ and $s = -2$ both lie to the right of the branch point for the square root function, which is located at $s = -9/4$. Hence they are contained within the closed integration contour C indicated in Figure 1. We can therefore use the residue theorem to write

$$\oint_C e^{sy} L(x, x_0, s) ds = 2\pi i \sum_{n=1}^2 \text{Res}(s_n), \quad (30)$$

where the left-hand side denotes the integral around the contour C and $\text{Res}(s_n)$ is the residue associated with the simple pole located at $s = s_n$, with $s_1 = 0$ and $s_2 = -2$. Note that the integration contour must avoid the branch cut of the square root function, extending from $s = -9/4$ to $s = -\infty$. Asymptotic analysis indicates that the contributions to the integral along the large arcs MN and QR vanish in the limit $r_1 \rightarrow \infty$ (see Fig. 1). Likewise, the integration along the small arc OP vanishes in the limit $r_2 \rightarrow 0$. Our solution for the energy distribution f_G therefore reduces to

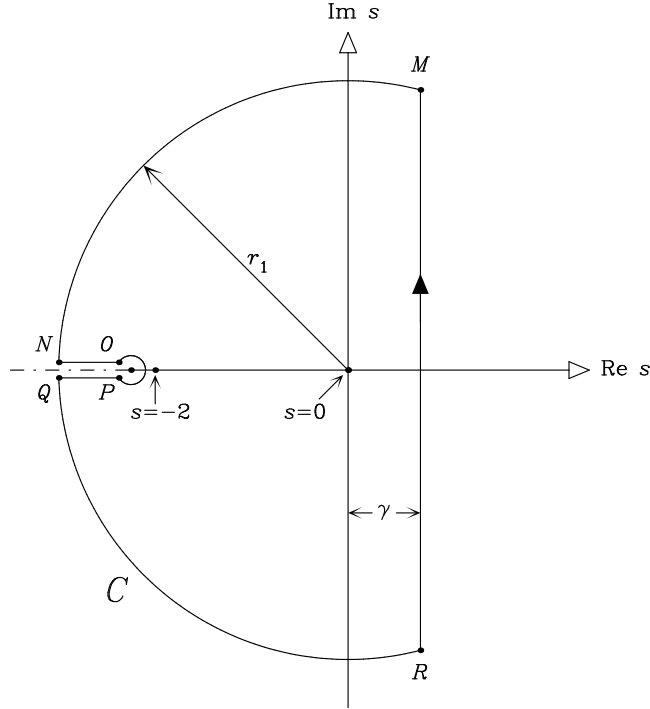


Figure 1. Closed integration contour C for the Laplace inversion integral on the left-hand side of equation (30). The branch point of the complex square root function is located at $s = -9/4$, in the center of the small arc OP , which has radius r_2 . Simple poles are located at $s = 0$ and $s = -2$; these singularities are contained within the contour C provided $\gamma > 0$. The branch cut (dot-dashed line) extends from the branch point to $s = -\infty$. See the discussion in the text.

$$f_G(x, x_0, y) = -\frac{1}{2\pi i} \int_N^O e^{sy} L(x, x_0, s) ds - \frac{1}{2\pi i} \int_P^Q e^{sy} L(x, x_0, s) ds + \sum_{n=1}^2 \text{Res}(s_n), \quad (31)$$

in the limit $r_1 \rightarrow \infty$, $r_2 \rightarrow 0$. Equation (31) expresses the Laplace inversion in terms of two residues and two integrals, one above the branch cut and one below it.

The residues appearing in equation (31) are evaluated in Appendix A.2, where we find that (see eqs. [A18])

$$\sum_{n=1}^2 \text{Res}(s_n) = \frac{e^{-x}}{2} + \frac{e^{-x-2y}}{2} \frac{(2-x)(2-x_0)}{x_0 x}. \quad (32)$$

The procedure for treating the integrations above and below the branch cut is discussed in Appendix A.3. This involves the utilization of symmetry relations and other identities satisfied by the Whittaker functions. The final result given by equation (A29) is

$$f_G(x, x_0, y) = \frac{32}{\pi} e^{-9y/4} x_0^{-2} x^{-2} e^{(x_0-x)/2} \int_0^\infty e^{-u^2 y} \frac{u \sinh(\pi u)}{(1+4u^2)(9+4u^2)} \\ \times W_{2, iu}(x_0) W_{2, iu}(x) du + \frac{e^{-x}}{2} + \frac{e^{-x-2y}}{2} \frac{(2-x)(2-x_0)}{x_0 x}. \quad (33)$$

This solution for the Green's function is one of the main results of the paper. It represents the fundamental “kernel” for the process of thermal Comptonization in an infinite homogeneous medium, from which particular solutions for any distribution of photon sources can be developed by quadrature. Spatial effects in a finite medium can be incorporated using the separation solution given by equation (15). In Appendix A.4, we provide the series expansions needed to evaluate the Whittaker functions in equation (33). Furthermore, a self-contained FORTRAN code that evaluates the Green's function by performing the integration in equation (33) is available from the author upon request. In the remainder of the paper, we will analyze the properties of the Green's function, and demonstrate that all of the previously known steady-state and time-dependent solutions can be reproduced using it. Hence equation (33) represents a significant generalization of the earlier analytical results in the theory of time-dependent thermal Comptonization.

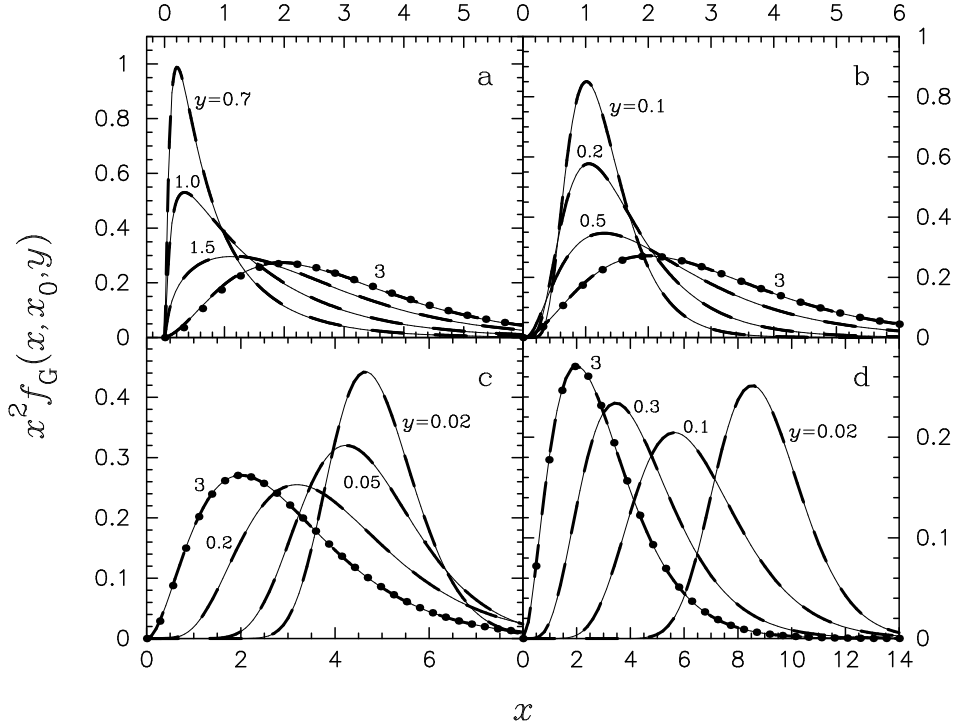


Figure 2. Analytical solution for the Green's function $x^2 f_G(x, x_0, y)$ (eq. [33]; solid lines) plotted as a function of the dimensionless photon energy x for the indicated values of the dimensionless time y . The area under each curve is equal to unity, and the initial photon energy is given by (a) $x_0 = 0.1$; (b) $x_0 = 1$; (c) $x_0 = 5$; and (d) $x_0 = 10$. Included for comparison are the numerical solutions (dashed lines) obtained by integrating numerically the Kompaneets equation using a Gaussian initial condition, as explained in the text. The two sets of curves are essentially identical. As y increases, $x^2 f_G(x, x_0, y)$ approaches the Wien spectrum $(1/2)x^2 e^{-x}$ (filled circles) in each case as expected.

3.3 Approach to Wien equilibrium

In the time-dependent, isothermal Comptonization problem treated here, the Green's function must approach the Wien equilibrium spectrum, i.e.,

$$\lim_{y \rightarrow \infty} f_G(x, x_0, y) = f_W(x) \equiv \frac{1}{2} e^{-x}, \quad (34)$$

where the factor of 1/2 on the right-hand side is required in order to ensure that f_W satisfies the normalization condition

$$\int_0^{\infty} x^2 f_W(x) dx = 1, \quad (35)$$

in compliance with equation (18). Our solution for $f_G(x, x_0, y)$ expressed by equation (33) clearly satisfies equation (34), and therefore the Green's function exhibits the correct asymptotic behavior for large values of y . In Figure 2 we plot f_G as a function of the dimensionless photon energy x and the dimensionless time y for four values of the initial photon energy, $x_0 = 0.1$, $x_0 = 1$, $x_0 = 5$, and $x_0 = 10$. Also included for comparison is the Wien equilibrium spectrum, $f_W(x) = (1/2)e^{-x}$. Note that in each case, the Green's function approaches the Wien shape for large values of y as predicted. The spectrum depicted in Figure 2 describes the Comptonization of an intrinsically narrow line feature. Applications to the broad Fe K α lines observed in AGNs are discussed in § 6.

3.4 Comparison with numerical simulations

The acid test for our Green's function solution is provided by comparing it with the photon energy distribution obtained by solving numerically the Kompaneets partial differential equation (16). In addition to specifying the initial condition for the photon distribution, the numerical solution procedure also requires the imposition of boundary conditions for f_G at large and small values of x , for all values of y . Obviously, this information is not available a priori, and therefore we are forced to push the boundaries of the computational domain as far as possible away from the region of interest, so as to avoid contaminating the solution with imprecise boundary data. This requirement markedly reduces the efficiency of the numerical approach, since much of the computer time is spent on calculations outside the region of interest. We have performed numerical simulations

using the IMSL partial differential equation solving subroutine DMOLCH. The initial condition is specified as a narrow Gaussian feature, with selected values for the mean energy $\langle x \rangle$ and standard deviation σ . This initial condition approximates the δ -function distribution given by equation (17) when $x_0 = \langle x \rangle$ and $\sigma/\langle x \rangle \ll 1$. The analytical and numerical solutions for $f_G(x, x_0, y)$ are compared in Figure 2 for four different scenarios. In Figure 2a, we set $\langle x \rangle = 0.1$ and $\sigma = 0.01$; in Figure 2b we set $\langle x \rangle = 1.0$ and $\sigma = 0.01$; in Figure 2c we set $\langle x \rangle = 5.0$ and $\sigma = 0.05$; and in Figure 2d we set $\langle x \rangle = 10$ and $\sigma = 0.1$. The results are plotted for several values of y . Note that the numerical and analytical solutions are virtually indistinguishable, confirming that our closed-form expression (eq. [33]) is in fact an exact representation of the Green's function.

4 PROPERTIES OF THE GREEN'S FUNCTION

The solution we have obtained in § 3.2 for the Green's function $f_G(x, x_0, y)$ given by equation (33) has a number of interesting properties that are further explored in this section.

4.1 Moments of the Green's function

We can obtain additional insight into the behavior of the Green's function by focusing on the variation of the “power moments,” $I_n^G(y)$, defined by

$$I_n^G(y) \equiv \int_0^\infty x^n f_G(x, x_0, y) dx . \quad (36)$$

Although the results obtained below for $I_n^G(y)$ are valid for general real values of n , in our specific applications we shall focus on integral values, since these correspond to cases of special physical interest such as the “number moment” I_2^G introduced in equation (20), and the “energy moment” I_3^G discussed below. In the case of the Green's function, the initial values of the power moments at $y = 0$ are obtained by substituting equation (17) into equation (36), which yields

$$I_n^G(0) = x_0^{n-2} . \quad (37)$$

We can determine the subsequent evolution of $I_n^G(y)$ by operating on equation (33) with $\int_0^\infty x^n dx$. The result obtained is

$$\begin{aligned} I_n^G(y) = & \frac{32}{\pi} e^{-9y/4} x_0^{-2} e^{x_0/2} \int_0^\infty e^{-u^2 y} \frac{u \sinh(\pi u)}{(1+4u^2)(9+4u^2)} W_{2,iu}(x_0) \\ & \times \int_0^\infty e^{-x/2} x^{n-2} W_{2,iu}(x) dx du + \frac{\Gamma(n+1)}{2} + (2-n) \Gamma(n) e^{-2y} \left(\frac{1}{x_0} - \frac{1}{2} \right) , \end{aligned} \quad (38)$$

where we have interchanged the order of integration over u and x . The integration with respect to x converges provided $n > 1/2$, in which case we can use equation (7.621.11) from Gradshteyn & Ryzhik (1980) to find that

$$\begin{aligned} I_n^G(y) = & \frac{32 e^{-9y/4} e^{x_0/2}}{\pi x_0^2 \Gamma(n-2)} \int_0^\infty e^{-u^2 y} \frac{u \sinh(\pi u)}{(1+4u^2)(9+4u^2)} W_{2,iu}(x_0) \Gamma(n-1/2+iu) \\ & \times \Gamma(n-1/2-iu) du + \frac{\Gamma(n+1)}{2} + (2-n) \Gamma(n) e^{-2y} \left(\frac{1}{x_0} - \frac{1}{2} \right) . \end{aligned} \quad (39)$$

We shall examine the behavior of this general expression for several cases of special interest below.

4.2 Variation of the number and energy moments

We have established via integration of the Kompaneets equation (16) that $f_G(x, x_0, y)$ must satisfy the normalization condition (cf. eq. [18])

$$I_2^G(y) = \int_0^\infty x^2 f_G(x, x_0, y) dx = 1 \quad (40)$$

for all values of y , in agreement with the initial condition for $I_2^G(y)$ expressed by equation (37). As pointed out in § 2.2, this behavior is a consequence of the fact that Compton scattering conserves the photon number density. We can use equation (39) to confirm explicitly that this condition is actually satisfied by our solution for the Green's function. When $n = 2$, the integral in equation (39) vanishes due to the factor $\Gamma(n-2)$ in the denominator, and we obtain

$$I_2^G(y) = 1 , \quad (41)$$

in satisfaction of equation (40). We have therefore established that our Green's function solution conserves photons and is properly normalized. Next we focus on the variation of the “energy moment,”

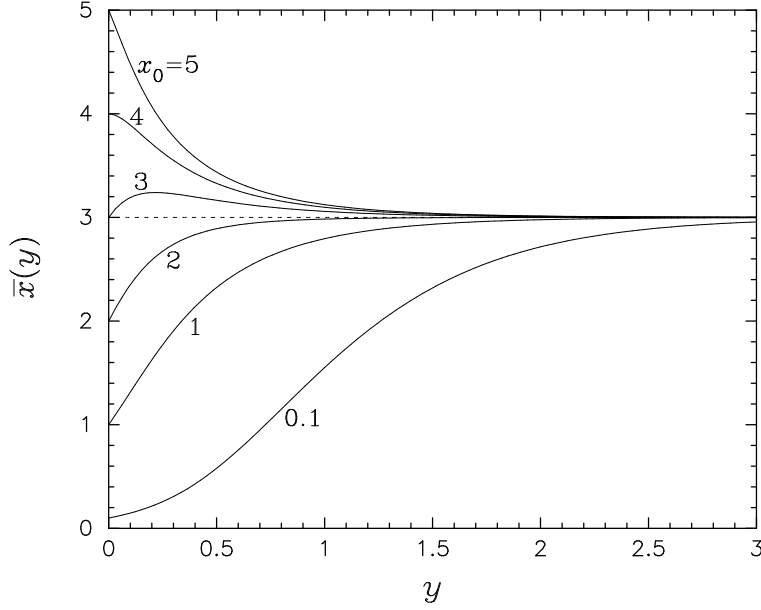


Figure 3. Mean photon energy \bar{x} for the case of a monoenergetic initial spectrum (eq. [46]), plotted as a function of the dimensionless time y for the indicated values of the initial photon energy x_0 . Note that in each case, $\bar{x} \rightarrow 3$ as $y \rightarrow \infty$ because the spectrum always equilibrates to the Wien form. The photons experience continual heating, on average, when $x_0 \leq 2$, and continual cooling when $x_0 \geq 4$. In the intermediate case with $2 < x_0 < 4$, a period of initial heating is followed by cooling. This behavior is a manifestation of the underlying variation of the spectral shape, as explained in the text.

$$I_3^G(y) \equiv \int_0^\infty x^3 f_G(x, x_0, y) dx, \quad (42)$$

which is related to the radiation energy density, U_r , via

$$U_r(\vec{r}, t) = \int_0^\infty \frac{8\pi}{c^3 h^3} \epsilon^3 \bar{n}(\epsilon, \vec{r}, t) d\epsilon = 8\pi \frac{(kT_e)^4}{(ch)^3} I_3^G(y). \quad (43)$$

Note that $I_3^G(y)$ is also equal to the mean photon energy, $\bar{x}(y)$, since

$$\bar{x}(y) \equiv \frac{\int_0^\infty x^3 f_G(x, x_0, y) dx}{\int_0^\infty x^2 f_G(x, x_0, y) dx} = I_3^G(y), \quad (44)$$

where the final result follows from equation (41). The variation of the mean photon energy was also considered by Kompaneets (1957), and we shall compare our result for $\bar{x}(y)$ with his. Setting $n = 3$ in equation (39) and using the identity

$$\Gamma(5/2 + iu)\Gamma(5/2 - iu) = \frac{\pi(1 + 4u^2)(9 + 4u^2)}{16 \cosh(\pi u)}, \quad (45)$$

we obtain for the variation of the mean photon energy

$$\bar{x}(y) = I_3^G(y) = 2x_0^{-2} e^{-9y/4} e^{x_0/2} \int_0^\infty e^{-u^2 y} W_{2, iu}(x_0) u \tanh(\pi u) du + 3 - 2e^{-2y} \left(\frac{1}{x_0} - \frac{1}{2} \right). \quad (46)$$

This result agrees with equation (48) from Kompaneets (1957), aside from the fact that his expression for $\bar{x}(y)$ contains an erroneous factor of $e^{-x_0/2}$ in place of the correct factor $e^{x_0/2}$ appearing in equation (46). In Figure 3 we plot the variation of $\bar{x}(y)$ as a function of y for several values of the initial photon energy x_0 . Note that in all cases, we find that $\bar{x}(0) = x_0$ initially, as required. For large values of y , we find that $\bar{x} \rightarrow 3$, as expected based on the fact that the photon distribution should approach the Wien spectrum $f_w(x) \propto e^{-x}$. However, the evolution of \bar{x} is not necessarily monotonic. For example, when $x_0 = 3$, the mean energy \bar{x} increases until $y \sim 0.25$, and then it decreases, asymptotically approaching the Wien value of 3 as $y \rightarrow \infty$. This behavior can be understood by examining the associated evolution of the inverse-Compton temperature, which we investigate in § 4.3.

4.3 Variation of the inverse-Compton temperature

By operating on the Kompaneets equation (16) with $\int_0^\infty x^n dx$ and integrating by parts twice, we can show that the power moments $I_n^G(y)$ satisfy the “differential recurrence relation”

$$\frac{dI_n^G}{dy} = (n-2) [(n+1)I_n^G(y) - I_{n+1}^G(y)] . \quad (47)$$

In particular, setting $n = 3$ yields the conservation equation for the energy moment $I_3^G(y) = \bar{x}(y)$,

$$\frac{dI_3^G}{dy} = 4I_3^G(y) \left[1 - \frac{T_{\text{IC}}(y)}{T_e} \right] , \quad (48)$$

where $T_{\text{IC}}(y)$ denotes the inverse-Compton temperature of the radiation field, defined by

$$\frac{T_{\text{IC}}(y)}{T_e} \equiv \frac{1}{4} \frac{I_4^G(y)}{I_3^G(y)} , \quad (49)$$

and

$$I_4^G(y) \equiv \int_0^\infty x^4 f_G(x, x_0, y) dx . \quad (50)$$

Equation (48) describes the conservation of total energy for a group of photons experiencing thermal Comptonization in a plasma with a Maxwellian electron distribution. When $T_{\text{IC}} < T_e$, the photons gain energy (\bar{x} increases), and \bar{x} decreases when $T_{\text{IC}} > T_e$. The inverse-Compton temperature varies in response to changes in the shape of the spectrum, and it does not necessarily track the behavior of \bar{x} . No net energy is exchanged between the radiation and the matter when $T_{\text{IC}} = T_e$, although subsequent evolution of the spectral shape can cause T_{IC} to move away from T_e . In the limit $y \rightarrow \infty$, we find that $T_{\text{IC}} \rightarrow T_e$ regardless of the initial energy of the photons because the spectrum asymptotically approaches the Wien form $f_W \propto e^{-x}$.

In the case of a monoenergetic initial spectrum, we can use equations (37) and (49) to conclude that the initial temperature ratio is given by

$$\frac{T_{\text{IC}}(0)}{T_e} = \frac{x_0}{4} . \quad (51)$$

Hence the photons will initially gain energy if $x_0 < 4$, and otherwise they will lose energy. The subsequent time evolution of $T_{\text{IC}}(y)$ can be determined by computing the variation of $I_4^G(y)$, which is accomplished by setting $n = 3$ in equation (47) and substituting for $I_3^G(y)$ using equation (46). The result obtained is

$$I_4^G(y) = \frac{e^{-9y/4} e^{x_0/2}}{2x_0^2} \int_0^\infty e^{-u^2 y} W_{2, iu}(x_0) u \tanh(\pi u) (25 + 4u^2) du + 12 - 12e^{-2y} \left(\frac{1}{x_0} - \frac{1}{2} \right) . \quad (52)$$

It is interesting to note that the same result can also be obtained by setting $n = 4$ in equation (39), which provides a useful check on the self-consistency of our formalism. Taken together, equations (46), (49), and (52) provide a new, closed-form solution describing the variation of the inverse-Compton temperature for an initially monoenergetic photon distribution. This result has not appeared previously in the literature, and it can be used to obtain additional physical insight into the energetics of thermal Comptonization, as discussed below. Our results for I_3^G and I_4^G confirm that $T_{\text{IC}}/T_e \rightarrow 1$ as $y \rightarrow \infty$, since $I_4^G \rightarrow 12$ and $I_3^G \rightarrow 3$. This behavior is consistent with our expectation that the spectrum should equilibrate to the Wien form.

In Figure 4 we plot the results obtained for $T_{\text{IC}}(y)$ by combining equations (46), (49), and (52) for several different values of the initial photon energy x_0 . There are a number of interesting features in the plots. First, note that for the cases with $x_0 < 4$, the photons are initially cooler than the electrons (see eq. [51]), and this explains the initial increase in the mean energy \bar{x} displayed in Figure 3. Conversely, when $x_0 > 4$, energy is initially transferred from the photons to the electrons, and therefore \bar{x} decreases. Note, however, that the variations of $\bar{x}(y)$ and $T_{\text{IC}}(y)$ are not necessarily monotonic. For example, the case with $x_0 = 3$ displays initial heating, and \bar{x} reaches a peak at $y \sim 0.25$. Beyond this point, the inverse-Compton temperature exceeds T_e , and the photons begin to lose energy. This is a consequence of the fact that \bar{x} must eventually decrease to the Wien value of 3 as $y \rightarrow \infty$, and this decrease can only happen if $T_{\text{IC}} > T_e$. Ultimately, T_{IC} approaches T_e and equilibrium is achieved. Hence the behaviors of T_{IC} and \bar{x} are fundamentally driven by the underlying evolution of the radiation spectrum.

For initial photon energies in the range $4 < x_0 < 6$, equation (51) indicates that T_{IC} exceeds T_e initially, and therefore the photons must lose energy to the electrons. However, despite the fact that \bar{x} is initially decreasing, we observe that T_{IC} actually proceeds to *increase*. This apparently paradoxical behavior stems from the variation of the spectral shape. We can obtain some useful insight into this phenomenon by computing the initial value of the temperature derivative, dT_{IC}/dy , in the case of a monoenergetic initial spectrum. By differentiating equation (49) with respect to y and using equation (47) to evaluate the derivatives of the moments, we find that for general values of y ,

$$\frac{d}{dy} \frac{T_{\text{IC}}(y)}{T_e} = \frac{3}{2} \frac{I_4^G}{I_3^G} - \frac{1}{2} \frac{I_5^G}{I_3^G} + \frac{1}{4} \left(\frac{I_4^G}{I_3^G} \right)^2 . \quad (53)$$

The initial value of the temperature derivative at $y = 0$ can be obtained by using equation (37) to substitute for the moments, which yields

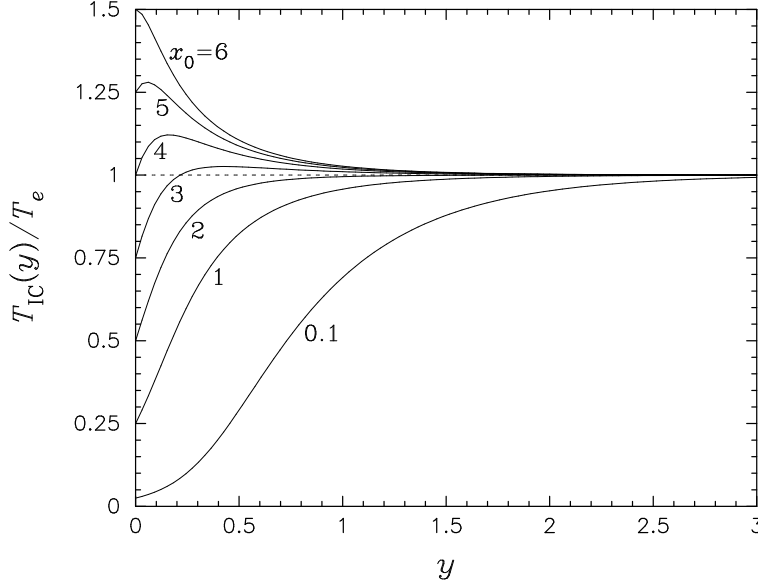


Figure 4. Inverse-Compton temperature ratio $T_{\text{IC}}(y)/T_e = (1/4) I_4^{\text{G}}(y)/I_3^{\text{G}}(y)$ plotted as a function of y for the case of a monoenergetic initial spectrum with the indicated value of the initial photon energy x_0 . The functions $I_3^{\text{G}}(y)$ and $I_4^{\text{G}}(y)$ are evaluated using equations (46) and (52), respectively. The inverse-Compton temperature increases initially if $x_0 < 6$.

$$\left. \frac{d}{dy} \frac{T_{\text{IC}}(y)}{T_e} \right|_{y=0} = \frac{x_0}{4} (6 - x_0). \quad (54)$$

This result clearly demonstrates that the inverse-Compton temperature T_{IC} initially increases if and only if $x_0 < 6$. On the other hand, according to equations (48) and (51), the mean photon energy \bar{x} initially increases if and only if $x_0 < 4$. Hence there is an intermediate regime, $4 < x_0 < 6$, within which \bar{x} initially decreases, while T_{IC} simultaneously increases. This illustrates the fact that \bar{x} and T_{IC} are not directly connected, but each is determined by the underlying evolution of the spectral shape, which is governed by the Kompaneets equation.

4.4 Particular solution for Wien initial spectrum

The Green's function solution given by equation (33) can be used to obtain the particular solution $f(x, y)$ corresponding to any desired initial spectrum $f_0(x)$. As discussed in § 2.2, the particular solution is given by the convolution

$$f(x, y) = \int_0^\infty x_0^2 f_0(x_0) f_{\text{G}}(x, x_0, y) dx_0. \quad (55)$$

The Wien initial spectrum,

$$f_0(x) = e^{-x}, \quad (56)$$

is a case of special interest, since it represents the equilibrium solution to the Kompaneets equation (16). Substituting equation (56) into equation (55) and evaluating $f_{\text{G}}(x, x_0, y)$ using equation (33), we obtain after interchanging the order of integration over x_0 and u

$$f(x, y) = e^{-x} + \frac{32}{\pi} e^{-9y/4} x^{-2} e^{-x/2} \int_0^\infty e^{-u^2 y} \frac{u \sinh(\pi u)}{(1 + 4u^2)(9 + 4u^2)} W_{2, iu}(x) \int_0^\infty e^{-x_0/2} W_{2, iu}(x_0) dx_0 du. \quad (57)$$

The integration over x_0 in equation (57) can be performed using equation (7.621.11) from Gradshteyn & Ryzhik (1980), which yields zero. The particular solution in the case of the Wien initial spectrum therefore reduces to

$$f(x, y) = e^{-x}, \quad (58)$$

which confirms that the Wien spectrum remains unaffected by isothermal Comptonization, as expected.

4.5 Particular solution for bremsstrahlung initial spectrum

The reprocessing of optically thin bremsstrahlung emission in clouds of hot electrons is thought to play a major role in the formation of the X-ray spectra observed during intense AGN flares (Lightman, Giacconi, & Tananbaum 1978). Becker &

Begelman (1986) and Chapline & Stevens (1973) studied this process by analyzing the evolution of an initial spectrum of the form

$$f_0(x) = x^{-3} e^{-x} . \quad (59)$$

The exact particular solution to this problem is given by Becker & Begelman as

$$f_{\text{BB}}(x, y) \equiv x^{-3} e^{-x} \left\{ 1 + \frac{3}{2} (1 - e^{-2y}) x + \frac{3}{2} [1 - e^{-2y} (2y + 1)] x^2 + \frac{3}{2} [y - 1 + e^{-2y} (y + 1)] x^3 \right\} . \quad (60)$$

This solution demonstrates the distortion produced by electron scattering, and the development of a thermal peak in the spectrum. However, due to the fact that the initial spectrum contains an infinite number of low-energy photons in this case, it is not possible to achieve full equilibration to a Wien distribution even in the limit $y \rightarrow \infty$. This unphysical behavior is an artifact of the utilization of equation (59) to describe the initial spectrum all the way down to zero energy. In an actual astrophysical situation, self-absorption effectively introduces a low-energy cutoff in the initial spectrum, as discussed below.

During intense AGN flares, soft seed photons produced in a relatively dense source region via bremsstrahlung are thought to be reprocessed in a corona containing hot electrons, in which scattering dominates over photon creation and destruction (Sunyaev & Titarchuk 1980; Nandra 2001). However, for photon energies below some critical energy x_* , the mean free path for free-free absorption in the source region becomes smaller than the size of the source. If the source region is homogeneous, then we can use the usual formulas for thermal bremsstrahlung to show that (Rybicki & Lightman 1979)

$$\frac{x_*^3}{1 - e^{-x_*}} = 6.6 \frac{U_r}{aT^4} , \quad (61)$$

where T and U_r denote the gas temperature and radiation energy density in the source region, respectively, and aT^4 is the blackbody energy density. In the physical applications of interest here, $U_r \ll aT^4$, and therefore we can rewrite equation (61) as

$$x_* = 2.6 \left(\frac{T_{\text{eff}}}{T_e} \right)^2 \ll 1 , \quad (62)$$

where $T_{\text{eff}} = (U_r/a)^{1/4}$ is the effective temperature of the radiation in the source region. Below the critical energy x_* , the initial spectrum given by equation (60) transitions into a Planck distribution at temperature T due to self-absorption. Since the number of photons per unit frequency range contained in the Planck distribution is proportional to the frequency ν as $\nu \rightarrow 0$, this effectively introduces a cutoff in the initial spectrum at energy $x = x_*$. The existence of this low-energy cutoff has a profound effect on the spectral evolution in the scattering region because the number of photons contained in the initial spectrum is now *finite*.

With the availability of our analytical expression for the Green's function given by equation (33), we are in a position to improve the situation by treating an optically thin bremsstrahlung initial spectrum that includes a low-energy cutoff. Specifically, we shall analyze the evolution of the “modified” bremsstrahlung initial spectrum given by

$$f_0(x) = \begin{cases} 0 , & x < x_* , \\ x^{-3} e^{-x} , & x \geq x_* , \end{cases} \quad (63)$$

where $x_* < 1$ denotes the low-energy cutoff, which approximates the effect of self-absorption. The number moment associated with this initial spectrum is (see eq. [20])

$$I_2 = \int_0^\infty x^2 f_0(x) dx = \Gamma(0, x_*) , \quad (64)$$

where $\Gamma(a, z)$ denotes the incomplete gamma function (Abramowitz & Stegun 1970). Note that the modified bremsstrahlung initial spectrum contains a finite number of photons. Combining equations (33), (55), and (63), and interchanging the order of integration over x_0 and u , we obtain

$$f(x, y) = \frac{32}{\pi} e^{-9y/4} x^{-2} e^{-x/2} \int_0^\infty e^{-u^2 y} \frac{u \sinh(\pi u)}{(1 + 4u^2)(9 + 4u^2)} W_{2, iu}(x) \int_{x_*}^\infty x_0^{-3} e^{-x_0/2} W_{2, iu}(x_0) dx_0 du + S , \quad (65)$$

where

$$S \equiv \frac{1}{2} e^{-x} \Gamma(0, x_*) + e^{-x-2y} \left(\frac{1}{x} - \frac{1}{2} \right) [2\Gamma(-1, x_*) - \Gamma(0, x_*)] . \quad (66)$$

The integration over x_0 in equation (65) can be worked out by employing equation (13.1.33) from Abramowitz & Stegun (1970) and equation (3.2.12) from Slater (1960) and integrating by parts three times. After some simplification, we obtain for the particular solution

$$f(x, y) = \frac{32}{\pi} e^{-9y/4} x^{-2} x_*^{-2} e^{-(x+x_*)/2} \int_0^\infty e^{-u^2 y} \frac{u \sinh(\pi u)}{(1 + 4u^2)(9 + 4u^2)} W_{2, iu}(x) \\ \times [W_{1, iu}(x_*) - 3W_{0, iu}(x_*) + 6W_{-1, iu}(x_*) - 6W_{-2, iu}(x_*)] du + S . \quad (67)$$

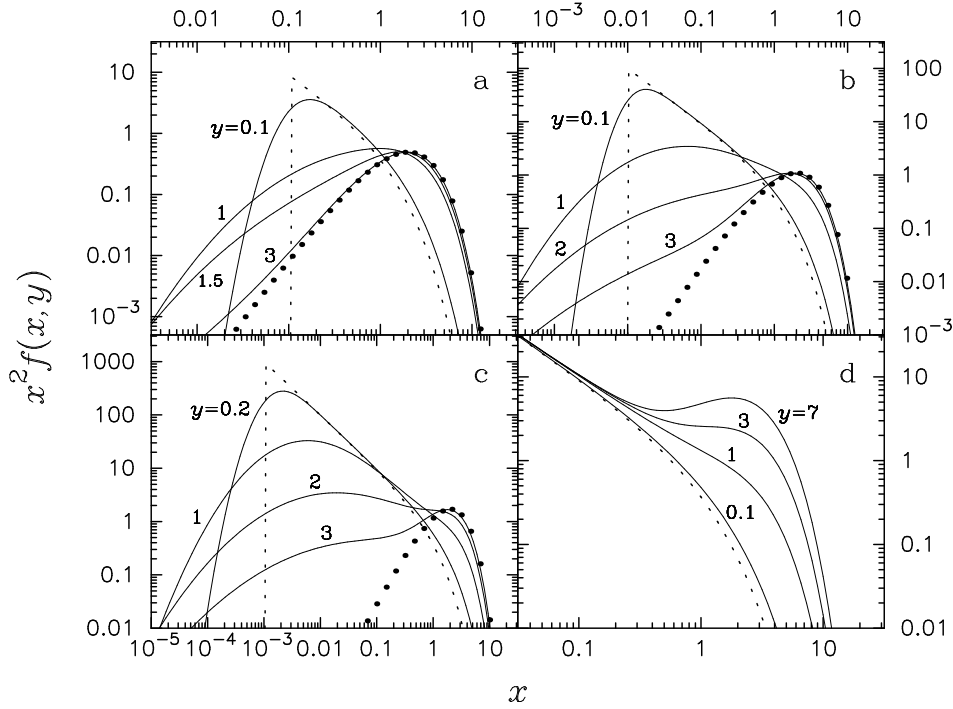


Figure 5. Time-dependent photon energy distribution $x^2 f(x, y)$ resulting from the Comptonization of the modified bremsstrahlung initial spectrum (eq. [67]; solid lines) plotted as a function of x for the indicated values of the dimensionless time y . Also included for comparison are the corresponding initial spectra (eq. [63]; dotted lines) and the equilibrium Wien spectra (filled circles). The values for the low-energy cutoff in the initial spectrum are (a) $x_* = 10^{-1}$; (b) $x_* = 10^{-2}$; (c) $x_* = 10^{-3}$; (d) $x_* = 0$. In panel (d), we have used equation (60) to evaluate $x^2 f$, and the Wien spectrum has been omitted since it does not exist in this case. The solutions in panels (a) - (c) show proper equilibration to the Wien spectrum as y increases, whereas the distribution in panel (d) does not due to the infinite number of photons in the initial spectrum.

This result describes the time-dependent Comptonization of an optically thin bremsstrahlung initial spectrum with a low-energy cutoff at $x = x_*$ and a finite number of photons. Note that as $y \rightarrow \infty$, the integral vanishes and $S \rightarrow \Gamma(0, x_*) e^{-x}/2$, and therefore we find that

$$\lim_{y \rightarrow \infty} f(x, y) = \frac{1}{2} e^{-x} \Gamma(0, x_*) = \frac{I_2}{2} e^{-x}, \quad (68)$$

where $I_2 = \Gamma(0, x_*)$ according to equation (64). Hence our solution clearly equilibrates asymptotically to the Wien spectrum $f_W(x) = (I_2/2) e^{-x}$, which satisfies the normalization requirement $\int_0^\infty x^2 f_W(x) dx = I_2$. Series expansions useful for evaluating the Whittaker functions appearing in equation (67) are provided in Appendix A.4, and a self-contained FORTRAN code that performs the integration to determine $f(x, y)$ is available from the author upon request.

The particular solution given by equation (67) represents a generalization of the $x_* = 0$ result $f_{\text{BB}}(x, y)$ (eq. [60]), and we find that

$$\lim_{x_* \rightarrow 0} f(x, y) = f_{\text{BB}}(x, y), \quad (69)$$

as required. In Figure 5 we use equation (67) to plot $f(x, y)$ for several values of the low-energy cutoff x_* . We also depict the equilibrium Wien spectrum $f_W(x) = (I_2/2) e^{-x}$, with $I_2 = \Gamma(0, x_*)$. As expected, the solutions with nonzero values of x_* are able to fully equilibrate to the Wien spectrum because the number of low-energy photons is finite in these cases. Equilibration occurs more rapidly as x_* is increased. Also included for comparison is the solution $f_{\text{BB}}(x, y)$ corresponding to $x_* = 0$, with an infinite number of photons (eq. [60]). In this case, the spectrum is unable to equilibrate. Our new solution for $f(x, y)$, given by equation (67), therefore displays a more reasonable physical behavior, and consequently it provides a rigorous basis for models of the X-ray spectral evolution during AGN flares. In § 5 we discuss the results obtained when equation (67) is coupled with a spatial transport model.

5 MODELS INCLUDING PHOTON ESCAPE

The Green's function solution obtained in § 3 describes the evolution of the photon energy distribution $f_G(x, x_0, y)$, but it does not address spatial issues such as the distribution of photons within the scattering cloud. In order to obtain the Green's

function for the occupation number, $\bar{n}_G(x, x_0, \vec{r}, \vec{r}_0, y)$, we must solve the spatial diffusion equation (13) for the radiation number density $\eta(\vec{r}, \vec{r}_0, y)$, and combine this information with $f_G(x, x_0, y)$ using equation (15). However, in many applications the detailed spatial distribution is not needed, and in such cases one may simply integrate over the volume of the cloud to describe the radiation spectrum as a function of energy and time only. In this section we take the latter approach and incorporate spatial effects by using a simple escape-probability formalism that serves to illustrate the general concept. More complex models with realistic geometries can easily be accommodated within our framework, provided the electron distribution in the cloud is homogeneous, as we have assumed.

5.1 Escape time distribution

Let us suppose that N_0 photons are injected into the cloud with an arbitrary spatial distribution at time $t = t_0$. Then the probability that a randomly-selected photon still remains inside the cloud at time $t \geq t_0$ is given by the escape time distribution

$$P(t) = \frac{N_r(t)}{N_0}, \quad (70)$$

where

$$N_r(t) = \oint_V n_r(\vec{r}, t) d^3\vec{r} \quad (71)$$

denotes the number of photons contained inside the cloud at time t , which is computed by integrating the radiation number density n_r over the volume V of the cloud. It follows that $P(t)$ decreases monotonically as a function of time from unity at $t = t_0$ to zero as $t \rightarrow \infty$ due to the escape of photons from the cloud.

In a homogeneous plasma, the energy and spatial distributions evolve in a decoupled manner as demonstrated in § 2.2. The probability that a photon randomly selected from the N_0 photons injected at time $t = t_0$ will subsequently escape in the time interval between t and $t + dt$ can be expressed as

$$P(t) \frac{dt}{t_{\text{esc}}} = -\frac{1}{N_0} \frac{dN_r}{dt} dt, \quad (72)$$

where the escape probability distribution $P(t)$ is given by equation (70), and

$$t_{\text{esc}}(t) = -\left(\frac{1}{P} \frac{dP}{dt}\right)^{-1} \quad (73)$$

represents the mean escape time for photons remaining in the cloud at time t . Note that $P(t) dt/t_{\text{esc}}$ is also equal to the fraction of the initial photons escaping between times t and $t + dt$. It is important to emphasize that, in general, the mean escape time t_{esc} varies as a function of time t due to the evolving nature of the photon distribution inside the cloud, which is a result of spatial diffusion. This variation can occur even when the electron distribution in the cloud is homogeneous, as assumed here. By virtue of equation (72), $P(t)$ clearly satisfies the normalization requirement

$$\int_{t_0}^{\infty} P(t) \frac{dt}{t_{\text{esc}}} = 1, \quad (74)$$

since $N_r(t_0) = N_0$. Once the radiation number density distribution $n_r(\vec{r}, t)$ has been determined by solving the appropriate diffusion equation, the escape probability $P(t)$ can be evaluated using equations (70) and (71). The result obtained for $n_r(\vec{r}, t)$ will naturally depend on the shape of the cloud and also on the initial spatial distribution of the photons at time $t = t_0$. Consequently, these factors will also influence the escape time distribution $P(t)$. Interested readers can find further details in Sunyaev & Titarchuk (1980).

Let us suppose that $P(t)$ has been computed in a given situation, and that the particular solution for the photon energy distribution $f(x, y)$ has also been determined by utilizing equation (19). In this case, the spectrum of the radiation remaining in the plasma at time t can be obtained by forming the product of f with the probability distribution P . Specifically, we find that the number of photons with dimensionless energy between x and $x + dx$ still residing within the cloud at time t is given by

$$N_x(x, t) dx \equiv P(t) x^2 f(x, y) dx, \quad (75)$$

where $y(t) = (t - t_0)n_e\sigma_T c(kT_e/m_e c^2)$ (see eq. [11]). Integration of N_x with respect to energy yields the total number of photons in the cloud,

$$N_r(t) = \int_0^{\infty} N_x(x, t) dx. \quad (76)$$

The number of photons with energy between x and $x + dx$ escaping from the cloud in the time interval between t and $t + dt$ is then given by

$$\dot{N}_x(x, t) dt dx \equiv t_{\text{esc}}^{-1} N_x(x, t) dt dx = t_{\text{esc}}^{-1} P(t) dt x^2 f(x, y) dx . \quad (77)$$

In § 4 we obtained particular solutions $f(x, y)$ corresponding to several specific initial spectra. The associated results for the escaping radiation spectrum \dot{N}_x are discussed below.

5.2 Escaping spectrum for monoenergetic initial condition

In order to demonstrate the effects of spatial transport without undue complexity, we shall assume here that $t_{\text{esc}} = \text{constant}$. This implies that the spatial distribution of the photon sources is proportional to the first eigenfunction of the diffusion operator, as discussed by Sunyaev & Titarchuk (1980). The specific result obtained for the initial density distribution in the spherical, homogeneous case with $t_{\text{esc}} = \text{constant}$ is

$$n_r(r, t) \Big|_{t=t_0} = \frac{N_0 \lambda^2}{\sin(\lambda R/\ell) - (\lambda R/\ell) \cos(\lambda R/\ell)} \frac{\sin(\lambda r/\ell)}{4\pi \ell^2 r} , \quad (78)$$

where N_0 is the total number of photons in the initial distribution, R is the radius of the cloud, $\ell = (n_e \sigma_T)^{-1}$ is the (constant) mean free path for electron scattering, and the eigenvalue λ is the smallest positive root of the equation

$$\tan\left(\frac{\lambda R}{\ell}\right) = \left(\frac{\lambda R}{\ell}\right) \left(1 - \frac{\tilde{\alpha} R}{\ell}\right)^{-1} . \quad (79)$$

The quantity $\tilde{\alpha}$ introduced in equation (79) is a constant of order unity that depends on the precise manner in which the flux boundary condition is specified at the surface of the cloud using the Eddington approximation. For example, Rybicki & Lightman (1979) set $\tilde{\alpha} = 3^{1/2}$ in their equation (1.124), whereas Sunyaev & Titarchuk set $\tilde{\alpha} = 3/2$ in their equation (A.3).

As t increases from the initial time t_0 , photons escape from the cloud due to spatial diffusion. The resulting time-dependent solution for the radiation number density is given by

$$n_r(r, t) = n_r(r, t_0) e^{-(t-t_0)/t_{\text{esc}}} , \quad (80)$$

where $n_r(r, t_0)$ is the initial distribution [eq. (78)] and

$$t_{\text{esc}} = \frac{3\ell}{\lambda^2 c} = \text{constant} \quad (81)$$

denotes the mean escape time. The probability that a photon injected at time t_0 still remains within the cloud at time t is therefore given by

$$P(t) = e^{-(t-t_0)/t_{\text{esc}}} . \quad (82)$$

We can now use equation (75) to express the number of photons with dimensionless energy between x and $x + dx$ residing within the cloud at time t as

$$N_x(x, t) dx = e^{-(t-t_0)/t_{\text{esc}}} x^2 f(x, y) dx , \quad (83)$$

where $y(t) = \tilde{y}(t - t_0)/t_{\text{esc}}$, and

$$\tilde{y} \equiv t_{\text{esc}} n_e \sigma_T c \frac{kT_e}{m_e c^2} = \text{Max}(\tau, \tau^2) \frac{kT_e}{m_e c^2} \quad (84)$$

represents the mean value of the Compton y -parameter experienced by photons before escaping from a cloud with scattering optical thickness $\tau = R/\ell$ (Rybicki & Lightman 1979). When $\tilde{y} \gtrsim 1$, significant Comptonization occurs before most of the radiation has escaped. In the limit of small \tilde{y} , little change in spectral shape occurs during the transient. The number of photons with energy between x and $x + dx$ escaping from the cloud in the time interval between t and $t + dt$ can be written as (see eq. [77])

$$\dot{N}_x(x, t) dt dx = t_{\text{esc}}^{-1} e^{-(t-t_0)/t_{\text{esc}}} dt x^2 f(x, y) dx . \quad (85)$$

In Figure 6, we plot the escaping photon distribution $\dot{N}_x(x, t)$ evaluated using equation (85), with $f(x, y)$ set equal to the Green's function solution given by equation (33). Results are presented for two values of the initial energy x_0 and two values of the mean Compton parameter \tilde{y} . The curves depicted in Figure 6 represent the spectra that would be observed outside the cloud as the initial burst of monochromatic (e.g., iron line) radiation is reprocessed by electron scattering, and gradually escapes from the cloud. For small values of $t - t_0$, the escaping spectrum is narrow and centered on the initial energy x_0 since little scattering has occurred. At intermediate times, the spectrum is broadened and the detailed shape depends on the value of the initial energy x_0 . The photon distribution is characterized by spectral hardening for $x_0 \lesssim 3$ and by spectral softening for $x_0 \gtrsim 3$. For large values of $t - t_0$, the spectrum has a Wien shape with a low normalization because most of the radiation has escaped. Equilibration to the Wien spectrum occurs more rapidly as x_0 and/or \tilde{y} are increased.

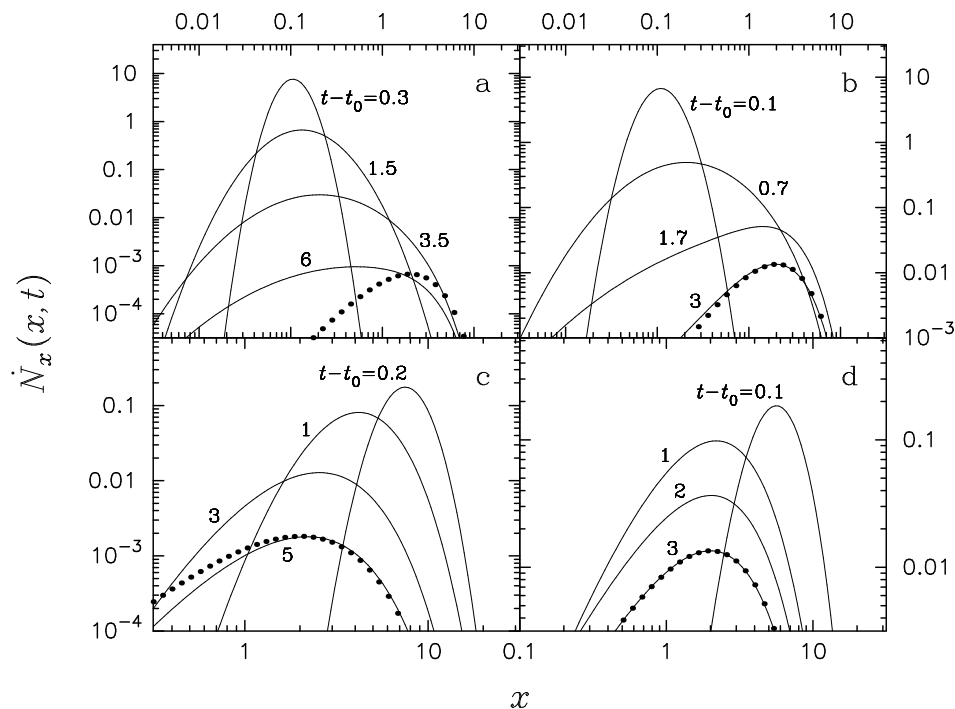


Figure 6. Time-dependent escaping photon distribution $\dot{N}_x(x, t)$ (eq. [85]; solid lines) plotted in units of t_{esc}^{-1} for the case of a spectrum that is initially monoenergetic at time $t = t_0$. The elapsed time $t - t_0$ in units of t_{esc} is indicated for each curve, and the values of the initial photon energy x_0 and the mean Compton parameter \tilde{y} (eq. [84]) are given by (a) $x_0 = 0.1$, $\tilde{y} = 0.2$; (b) $x_0 = 0.1$, $\tilde{y} = 1$; (c) $x_0 = 10$, $\tilde{y} = 0.2$; and (d) $x_0 = 10$, $\tilde{y} = 1$. The normalization of the curves decreases over time due to the loss of radiation from the scattering cloud, as described by equation (82). Included in each case is the Wien spectrum (filled circles) evaluated at time t_{max} , where t_{max} is the maximum time for the sequence of curves in the panel.

5.3 Escaping spectrum for bremsstrahlung initial condition

It is also interesting to examine the distribution of radiation escaping from the scattering cloud in the case of the modified bremsstrahlung initial spectrum given by equation (63). We shall again assume that $t_{\text{esc}} = \text{constant}$, and therefore we can employ equation (82) for the escape probability distribution P . In Figure 7, we plot the results for the escaping photon distribution $\dot{N}_x(x, t)$ computed using equation (85), with $f(x, y)$ set equal to the particular solution for the modified bremsstrahlung initial spectrum given by equation (67). Results are presented for two values of the low-energy cutoff x_* and two values of the mean Compton parameter \tilde{y} . For small values of $t - t_0$, the escaping spectrum resembles the initial distribution. At intermediate times, the spectrum displays the hardening that is characteristic of Comptonized bremsstrahlung, and as t increases, the spectrum approaches the Wien distribution. The details of the spectral evolution depend on the values of x_* and \tilde{y} , which may allow the extraction of these parameters from a sequence of spectra observed during a strong X-ray transient. For example, let us suppose that the transient begins with the impulsive injection into the corona of a pulse of soft bremsstrahlung radiation with an initial spectrum given by equation (63). As Figure 7 indicates, the shape of the spectrum for energies $x \lesssim 1$ at the time of appearance of the Wien peak, combined with the overall amplitude of the spectrum at that time, is a sensitive indicator of the unique values of x_* and \tilde{y} . In general, the low-energy spectrum increases with decreasing x_* because it takes longer for the additional soft photons to be upscattered, and the overall amplitude of the spectrum at the time of appearance of the Wien peak increases with increasing \tilde{y} due to the competition between Comptonization and photon escape. Indeed, the simple observation of a Wien peak in the escaping spectrum would indicate that $\tilde{y} \gtrsim 1$, since otherwise the peak would occur after the normalization had already declined by several orders of magnitude due to photon escape, rendering the Wien bump unobservable. Increasing either x_* or \tilde{y} results in more rapid equilibration to the Wien shape. The type of spectral evolution depicted in Figure 7 is expected to occur when the timescale for the impulsive injection of the bremsstrahlung radiation is shorter than the timescale for the radiation to escape from the cloud. In the next section we consider the situation with continual photon injection, resulting in the evolution of the spectrum towards a steady-state form.

5.4 Generation of the steady-state Green's function

The solution we have obtained for the Laplace transform $L(x, x_0, s)$ is closely related to the steady-state photon energy distribution resulting from the continual injection of monoenergetic radiation into a cloud of scattering electrons that is

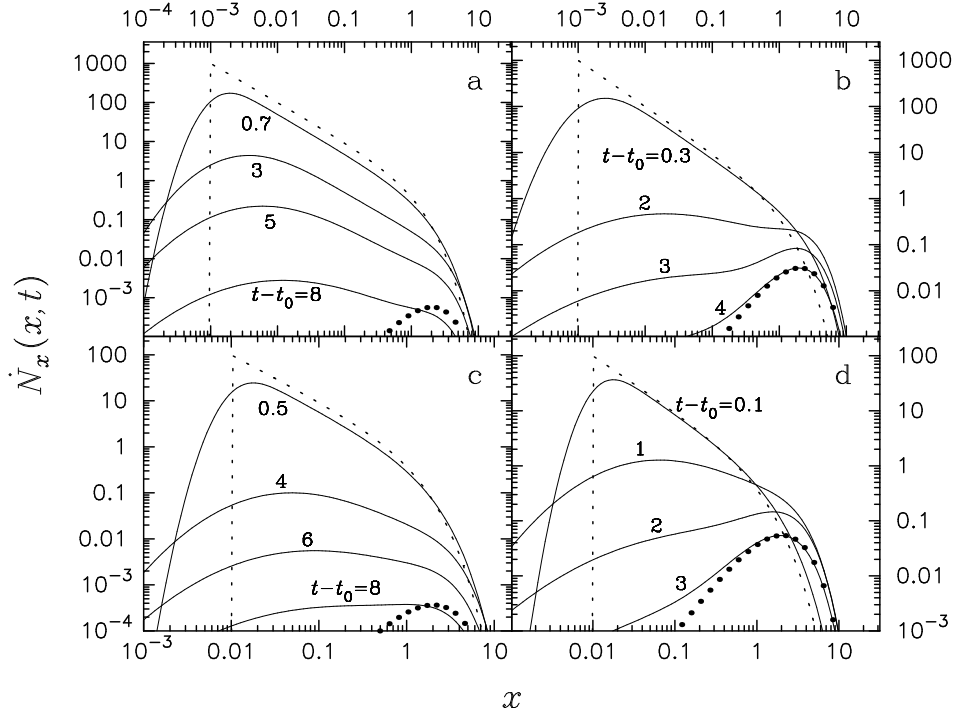


Figure 7. Time-dependent escaping photon distribution $\dot{N}_x(x, t)$ (eq. [85]; solid lines) plotted in units of t_{esc}^{-1} for the case of the modified bremsstrahlung initial spectrum (eq. 63; dotted lines). The elapsed time $t - t_0$ in units of t_{esc} is indicated for each curve, and the values of the low-energy cutoff x_* and the mean Compton parameter \tilde{y} are given by (a) $x_* = 10^{-3}$, $\tilde{y} = 0.2$; (b) $x_* = 10^{-3}$, $\tilde{y} = 1$; (c) $x_* = 10^{-2}$, $\tilde{y} = 0.2$; and (d) $x_* = 10^{-2}$, $\tilde{y} = 1$. Included for comparison in each case is the Wien spectrum (filled circles) evaluated at the time t_{max} , where t_{max} is the maximum time for the sequence of curves in the panel.

leaking photons into the surrounding space. In this section, we explore the connection in detail, and establish that our time-dependent Green's function solution can be used to generate the *steady-state* Green's function corresponding to a balance between photon injection, thermal Comptonization, and photon escape. The steady-state solution is one of the most important and widely applied spectral models in X-ray data analysis, and it successfully accounts for the formation of the power-law spectra commonly observed in the quiescent emission from galactic and extragalactic sources.

Let us suppose that the monoenergetic photon source is turned on at time $t = 0$. In this situation, the number spectrum of the photons remaining in the cloud at time t can be written in terms of the Green's function as the convolution

$$N_x(x, t) = \int_0^t \dot{N}_0 P(t) x^2 f_G(x, x_0, y) dt, \quad (86)$$

where \dot{N}_0 expresses the rate of injection of fresh photons with dimensionless energy x_0 into the cloud per unit time, and $y(t) = n_e \sigma_T c (kT_e / m_e c^2) (t - t_0)$ according to equation (11). The number spectrum $N_x(x, t)$ is related to the total number of photons in the cloud $N_r(t)$ via $N_r(t) = \int_0^\infty N_x(x, t) dx$ (see eq. [76]). Transforming the variable of integration in equation (86) from t_0 to $\xi \equiv (t - t_0) / t_{\text{esc}}$ and substituting for P using equation (82) yields

$$N_x(x, t) = \int_0^{t/t_{\text{esc}}} t_{\text{esc}} \dot{N}_0 e^{-\xi} x^2 f_G(x, x_0, \tilde{y} \xi) d\xi, \quad (87)$$

where $\tilde{y} = t_{\text{esc}} n_e \sigma_T c (kT_e / m_e c^2)$ (eq. [84]). The spectrum of the radiation escaping from the cloud is given by

$$\dot{N}_x(x, t) = \int_0^{t/t_{\text{esc}}} \dot{N}_0 e^{-\xi} x^2 f_G(x, x_0, \tilde{y} \xi) d\xi. \quad (88)$$

In the limit $t \rightarrow \infty$, a steady-state balance is obtained between monoenergetic photon injection, thermal Comptonization, and photon escape. The resulting steady-state spectrum of the escaping radiation, $\dot{N}_x^{\text{std}}(x)$, is given by

$$\dot{N}_x^{\text{std}}(x) = \lim_{t \rightarrow \infty} \dot{N}_x(x, t) = \int_0^\infty \dot{N}_0 e^{-\xi} x^2 f_G(x, x_0, \tilde{y} \xi) d\xi. \quad (89)$$

By construction, this represents the Green's function solution for the time-independent problem. Transformation of the variable of integration from ξ to $y = \tilde{y} \xi$ now yields

$$\dot{N}_x^{\text{std}}(x) = \frac{\dot{N}_0 x^2}{\tilde{y}} \int_0^\infty e^{-y/\tilde{y}} f_G(x, x_0, y) dy . \quad (90)$$

Comparing this expression with equation (22), we recognize that the integral on the right-hand side is simply the Laplace transformation of $f_G(x, x_0, y)$ with the complex variable s replaced by $1/\tilde{y}$. We can therefore immediately write

$$\dot{N}_x^{\text{std}}(x) = \frac{\dot{N}_0 x^2}{\tilde{y}} L\left(x, x_0, \frac{1}{\tilde{y}}\right) . \quad (91)$$

Substituting for $L(x, x_0, 1/\tilde{y})$ using equation (25) yields the equivalent result

$$\dot{N}_x^{\text{std}}(x) = \frac{\dot{N}_0}{\tilde{y}} \frac{\Gamma(\tilde{\mu} - 3/2)}{\Gamma(1 + 2\tilde{\mu})} x_0^{-2} e^{(x_0 - x)/2} M_{2, \tilde{\mu}}(x_{\min}) W_{2, \tilde{\mu}}(x_{\max}) , \quad (92)$$

where x_{\max} and x_{\min} are defined by equations (26), and

$$\tilde{\mu} \equiv \left(\frac{9}{4} + \frac{1}{\tilde{y}}\right)^{1/2} . \quad (93)$$

This is essentially the same solution to the stationary Kompaneets equation derived by Sunyaev & Titarchuk (1980) in their Appendix B if we set their separation constant $\gamma = 1/\tilde{y}$. The normalization of our solution for $\dot{N}_x^{\text{std}}(x)$ can be confirmed by integrating equation (92) to show that the total number of photons escaping from the cloud per unit time is given by

$$\int_0^\infty \dot{N}_x^{\text{std}}(x) dx = \dot{N}_0 , \quad (94)$$

as expected. Hence we have demonstrated that our solution for the time-dependent Green's function can be used to generate the steady-state Green's function. However, our solution also contains additional information describing the evolution of the spectrum towards the steady state, as discussed below.

5.5 Evolution towards the steady-state spectrum

We can use the results derived in § 5.4 to study the evolution of the photon distribution following the “turning on” of a continual source of monochromatic radiation at time $t = 0$. We assume that no photons are initially present in the cloud. This scenario describes, for example, an X-ray transient driven by the continual injection of iron line emission. Whether or not a steady state is established depends on whether the injection phase lasts longer than the characteristic timescale for the escape of radiation from the cloud. In Figure 8, we plot a sequence of curves describing the variation of the time-dependent escaping spectrum $\dot{N}_x(x, t)$ computed using equation (88), with $f_G(x, x_0, y)$ evaluated using equation (33). We also include the steady-state spectrum $\dot{N}_x^{\text{std}}(x)$ given by equation (92). Two different values of the initial photon energy x_0 and the mean Compton parameter \tilde{y} are considered. Note that as time increases, the spectrum broadens and the time-dependent curves approach the corresponding steady-state solutions as expected. The steady-state spectrum exhibits power-law wings around $x = x_0$ when $\tilde{y} \lesssim 1$ and $x_0 \lesssim 1$ (see Rybicki & Lightman 1979). For large values of x , the spectrum declines exponentially. The final equilibrium represents a balance between Comptonization, photon injection, and photon escape. The steady-state spectrum gives good agreement with the quiescent X-ray spectra observed from many active galaxies. However, with the availability of the new solution for the time-dependent Green's function, it is now possible to model the *transient* phase in the development of the steady-state spectrum using equation (88). This new theoretical framework improves our ability to interpret spectral/temporal data associated with flares that are driven by the injection of radiation on timescales shorter than that required for the establishment of a steady state.

6 CONCLUSIONS

In this paper, we have derived several new results of importance in the theory of time-dependent thermal Comptonization. The analysis is based on the transport equation (1), which describes the effects of energy diffusion (second-order Fermi energization), electron recoil, and spatial diffusion. The spatial and energetic components of the problem were separated by writing the Green's function for the occupation number \bar{n}_C as the product of the energy Green's function $f_G(x, x_0, y)$ and the spatial distribution $\eta(\vec{r}, \vec{r}_0, y)$ (eq. [15]), which is valid provided the scattering cloud has a steady, homogeneous structure. The Green's function \bar{n}_C represents the response of the system to the injection of a single photon with an arbitrary energy at an arbitrary time and location within the cloud. The particular solution for the occupation number distribution corresponding to a general source term can be obtained by integrating \bar{n}_C using equation (7).

The central result obtained in the subsequent analysis is the closed-form solution for the Kompaneets Green's function, $f_G(x, x_0, y)$, given by equation (33) and plotted in Figure 2. This fundamental expression describes the evolution of an initially

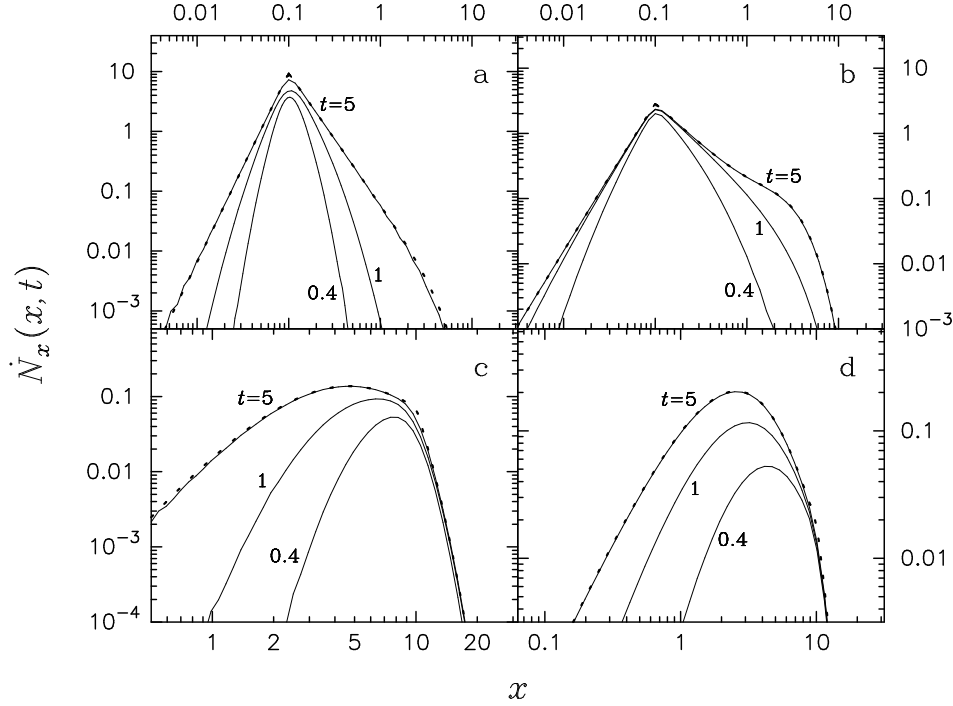


Figure 8. Time-dependent escaping photon distribution $\dot{N}_x(x, t)$ (eq. [88]; solid lines) plotted in units of the injection rate \dot{N}_0 for the indicated values of the elapsed time t in units of t_{esc} . The scenario considered here corresponds to the continual injection of monochromatic radiation with energy x_0 , beginning at time $t = 0$. The values of x_0 and the mean Compton parameter \tilde{y} are given by (a) $x_0 = 0.1$, $\tilde{y} = 0.2$; (b) $x_0 = 0.1$, $\tilde{y} = 1$; (c) $x_0 = 10$, $\tilde{y} = 0.2$; and (d) $x_0 = 10$, $\tilde{y} = 1$. As time increases, the spectrum broadens and the time-dependent curves approach the steady-state solution $\dot{N}_x^{\text{std}}(x)$ (eq. [92]; dashed lines).

monoenergetic radiation spectrum in an infinite medium under the influence of repeated Compton scattering. As such, it serves as the “kernel” for thermal Comptonization, from which one can obtain the particular solution for any distribution of photon sources in time, space, and energy. The validity of this new analytical solution was confirmed in § 3 via comparison with the results obtained for the energy spectrum by integrating numerically the Kompaneets equation (see Fig. 2). The availability of our closed-form solution for the Green’s function describing thermal Comptonization provides a valuable new tool for the analysis and interpretation of variable X-ray spectra. In particular, the Green’s function represents an efficient alternative to numerical integration of the Kompaneets equation that avoids the complications and uncertainties associated with the imposition of boundary conditions in the energy space.

The properties of the Green’s function were explored in detail in § 4, where we confirmed that it displays proper equilibration to the Wien spectrum at large times. We also reproduced Kompaneets’ result concerning the variation of the mean photon energy \bar{x} as a function of time (eq. [46]; Fig. 3), once a typographical error made by Kompaneets is taken into account. Furthermore, we obtained a new expression for the variation of the inverse-Compton temperature associated with a monoenergetic initial spectrum (Fig. 4), given by $T_{\text{IC}}/T_e = (1/4) I_4^G/I_3^G$, where the moments I_3^G and I_4^G are evaluated using equations (46) and (52), respectively. We also used our solution for the Green’s function to derive a new, exact expression for the spectrum resulting from the time-dependent Comptonization of a bremsstrahlung initial spectrum, including a low-energy cutoff that approximates the effect of self-absorption. The new solution equilibrates to the Wien spectrum at large times (see eq. [67] and Fig. 5).

Although the Green’s function $f_G(x, x_0, y)$ obtained here represents the solution to the Kompaneets equation in an infinite medium, the formalism we have developed can also incorporate the effects of spatial transport in a homogeneous scattering cloud of any size and shape. In § 5, modifications associated with spatial transport in a cloud of finite size were examined using a simple escape-probability model. In this scenario, photons injected into the cloud with energy x_0 at some initial time $t = t_0$ are subject to thermal Comptonization as they diffuse out of the cloud. The analytical result for the escaping radiation spectrum $\dot{N}_x(x, t)$ given by equation (85) was plotted for monoenergetic and bremsstrahlung initial spectra in Figures 6 and 7, respectively. We also analyzed the case of the *continual* injection of monoenergetic photons into a “leaky” cloud, starting at time $t = 0$. A new time-dependent solution describing the gradual build-up of the escaping radiation spectrum was obtained (eq. [88]), and it was explicitly confirmed that in the limit $t \rightarrow \infty$, the time-dependent spectrum approaches the steady-state solution given by Sunyaev & Titarchuk (1980), describing a balance between photon injection, thermal Comptonization, and photon escape (see eq. [92] and Fig. 8).

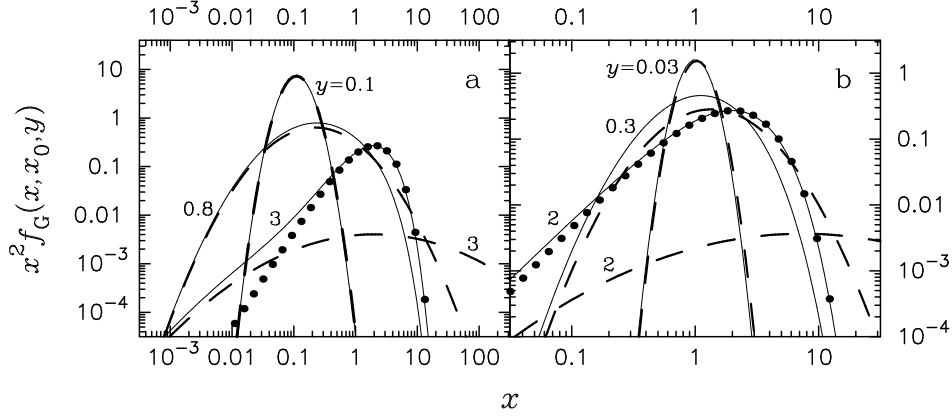


Figure 9. Exact Green's function $x^2 f_G(x, x_0, y)$ (eq. [33]; solid lines) plotted as a function of the dimensionless photon energy x for the indicated values of the dimensionless time y . The initial photon energy is given by (a) $x_0 = 0.1$ and (b) $x_0 = 1$. Included for comparison is the “soft-photon Green's function,” $x^2 f_{\text{soft}}(x, x_0, y)$ (eq. [98]; dashed lines), which ignores the recoil term in the Kompaneets equation (16), and therefore does not equilibrate to the Wien spectrum $(1/2)x^2 e^{-x}$ (filled circles) as $y \rightarrow \infty$. Conversely, $f_G(x, x_0, y)$ satisfies the complete Kompaneets equation, and therefore it approaches the Wien spectrum as y increases.

6.1 Relation to previous solutions

The new solution for the Green's function obtained in § 3.2 describes the fundamental physics of thermal Comptonization in a homogeneous plasma with steady properties. It therefore unifies and extends several of the previously known analytical solutions. For example, the new solution generalizes the analytical solution obtained by Zeldovich & Sunyaev (1969) and Payne (1980) for the Comptonization of soft photons with $x \ll 1$, which satisfies the equation

$$\frac{\partial f}{\partial y} = \frac{1}{x^2} \frac{\partial}{\partial x} \left(x^4 \frac{\partial f}{\partial x} \right). \quad (95)$$

This equation does not include the electron recoil term proportional to f that appears in the full Kompaneets equation (16), and therefore it only treats the stochastic energization of the photons. The exact solution to equation (95), which we refer to as the “soft-photon Green's function,” can be obtained using the Laplace inversion integral (eq. [29]) by working in the limit $x \ll 1$, $x_0 \ll 1$ (Titarchuk 2003, private communication). Along the inversion contour, $\text{Re } s = \gamma > 0$, and therefore it follows that $\text{Re } \mu > 0$ since $\mu = (s + 9/4)^{1/2}$ according to equation (24). The Whittaker functions $W_{2, \mu}(x)$ and $M_{2, \mu}(x)$ appearing in equation (25) for the Laplace transform $L(x, x_0, s)$ consequently have the leading behaviors (see eqs. [27] and [28])

$$M_{2, \mu}(x) \cong e^{-x/2} x^{\mu+1/2}, \quad W_{2, \mu}(x) \cong \frac{\Gamma(2\mu)}{\Gamma(\mu - 3/2)} e^{-x/2} x^{-\mu+1/2}, \quad (96)$$

for small x . Utilizing these asymptotic expressions for the Whittaker functions in equation (25), we find that the Laplace transform of the soft-photon Green's function is given by

$$L_{\text{soft}}(x, x_0, s) = \frac{(x_0 x)^{-3/2}}{2\mu} \left(\frac{x_{\min}}{x_{\max}} \right)^\mu, \quad (97)$$

where x_{\max} and x_{\min} are defined by equations (26). By performing the inverse Laplace transformation of L_{soft} using equation (29), we obtain for the soft-photon Green's function the solution

$$f_{\text{soft}}(x, x_0, y) = \frac{(x_0 x)^{-3/2} e^{-9y/4}}{2\sqrt{\pi y}} \exp \left[\frac{-(\ln x - \ln x_0)^2}{4y} \right], \quad (98)$$

which satisfies equation (95), as well as the initial condition (see eq. [17])

$$f_{\text{soft}}(x, x_0, y) \Big|_{y=0} = x_0^{-2} \delta(x - x_0). \quad (99)$$

Note that due to the neglect of the recoil effect, f_{soft} fails to equilibrate to the Wien distribution as $y \rightarrow \infty$. In Figure 9 we compare f_{soft} with the general Green's function f_G (eq. [33]) for two values of the initial photon energy, $x_0 = 0.1$ and $x_0 = 1$. At early times (i.e., small values of y), the two solutions agree closely. However, as y increases, strong disagreement becomes evident. In particular, at high energies (large x), the f_{soft} distribution continues to increase far beyond the saturation level indicated by the Wien spectrum. Conversely, our exact solution for f_G , which includes the effect of electron recoil, equilibrates to the Wien form as required, and it therefore generalizes the Zeldovich & Sunyaev (1969) and Payne (1980) solution.

In § 4.5 we considered the important problem of the Comptonization of a “modified” bremsstrahlung initial spectrum that includes a low-energy cutoff at energy $x = x_*$, which simulates the effect of self-absorption. Our new time-dependent

analytical solution for the resulting spectrum (eq. [67]) generalizes the analytical solution obtained by Chapline & Stevens (1973) and Becker & Begelman (1986), which sets the low-energy cutoff $x_* = 0$, and therefore contains an infinite number of low-energy photons. While the $x_* = 0$ solution cannot equilibrate to the Wien spectrum, our new solution satisfies this physical requirement, and it therefore represents a distinct improvement over the previously known analytical result for bremsstrahlung injection. We demonstrated in § 4.5 that the low-energy cutoff x_* and the mean value of the Compton y -parameter, \bar{y} , can be estimated from observations of a sequence of spectra obtained during a bremsstrahlung-driven X-ray flare. Knowledge of these quantities yields constraints relating the electron temperature T_e and optical thickness τ of the corona to the gas temperature T and effective temperature T_{eff} in the source region (see eqs. [62] and [84]).

The new solution for the Green's function obtained here also generalizes the steady-state solution derived by Sunyaev & Titarchuk (1980) through the inclusion of the full time dependence of the spectral evolution process. However, it should be pointed out that the Sunyaev & Titarchuk formalism is also applicable to the case of an inhomogeneous scattering cloud, whereas the time-dependent solution obtained in the present paper was developed under the assumption of a homogeneous electron distribution. In future work we intend to investigate the possibility of generalizing the time-dependent Green's function in order to treat the inhomogeneous case as well. This would be a significant improvement since observations suggest that the electron distribution is probably inhomogeneous in a number of X-ray sources, as discussed in § 6.2. We briefly review the potential astrophysical relevance of the results presented in this paper below.

6.2 Astrophysical relevance

The closed-form solution for the Green's function describing thermal Comptonization (eq. [33]) provides a useful new tool for the analysis and interpretation of variable X-ray spectra. Analytical solutions offer far more physical insight than do numerical simulations, and they also provide the flexibility to efficiently explore a large region of parameter space. The new solution is relevant in a wide variety of astrophysical situations involving thermal Comptonization, such as studies of the reprocessing of the cosmological background radiation (Shimon & Rephaeli 2002; Colafrancesco et al. 1997), models of thermal upscattering in gamma-ray bursts (Ghisellini & Celotti 1999; Liang et al. 1999), studies of variability and lags in the X-ray spectra observed from AGNs and galactic black-hole candidates (Zdziarski et al. 2002; Lee et al. 2000), spectral reprocessing in X-ray bursts (Titarchuk 1988; Lapidus, Sunyaev, & Titarchuk 1987), and the Comptonization of line features in AGN spectra (Misra & Kembhavi 1998; Wang et al. 1999). The solution presented here is also perfectly suited for modeling the acceleration of relativistic electrons in a turbulent plasma. In this application, the terms proportional to $\partial f_G/\partial x$ and f_G inside the parentheses on the right-hand side of equation (16) describe the second-order Fermi acceleration of the electrons and the effects of synchrotron/inverse-Compton losses, respectively (Schlickeiser, Sievers, & Thiemann 1987; Schlickeiser 1984; Lacombe 1977). The availability of our exact solution for the Green's function therefore provides a unique opportunity to model analytically the time-dependent development of the electron energy spectrum during solar flares and other high-energy astrophysical transients (e.g., Park, Petrosian, & Schwartz 1997; Miller & Ramaty 1989).

The best prospects for extragalactic, time-resolved X-ray spectroscopy of accretion flows around black holes are presented by nearby AGNs such as NGC 4051, NGC 4151, NGC 6814, and MCG-6-30-15, which are among the brightest and most strongly variable X-ray sources known. The rapid variability of these and other Seyfert galaxies represents one of the most interesting puzzles in modern X-ray astronomy. A large body of observational evidence suggests that as the 2-10 keV flux increases in these sources, the X-ray spectrum becomes softer (Lee et al. 2000; Merloni & Fabian 2001; Nandra 2001). For example, observations of the dwarf Seyfert nucleus of NGC 4395 reported by Iwasawa et al. (2000) reveal rapid variability, including flares during which the flux changes by a factor of 3-4 in a single half-day *ASCA* observation. Doubling times as short as 100 s have been observed. The highly variable Seyfert galaxy NGC 6814 has displayed factor of 3 changes in flux in 8 hours (König et al. 1997). The characteristic softening observed during the Seyfert flares may reflect inverse-Compton cooling of the corona due to the injection of copious soft photons (possibly due to bremsstrahlung) from the inner region of the accretion disk. The spectral evolution observed during these transients may provide us with a direct opportunity to study time-dependent Comptonization. However, it is also possible that the variable X-ray spectra may be more correctly interpreted using a sequence of steady-state models, if the timescale for the injection of the photons exceeds the characteristic time for the photons to diffuse out of the cloud (Sunyaev & Titarchuk 1980).

The signature of time-dependent Comptonization is perhaps most unambiguously observed in the complex cross-spectra produced by combining the Fourier transformed lightcurves at two different X-ray energies (van der Klis et al. 1987). The resulting structure of the X-ray time lags contains detailed information on the "Compton reverberations" taking place in the inner region of the disk/corona (Payne 1980; Reynolds et al. 1999) that cannot be obtained using standard analysis (Kazanas, Hua, & Titarchuk 1997). Observations of hard X-ray time lags in AGNs and galactic black-hole candidates are consistent with the predictions of thermal Comptonization models (Zdziarski et al. 2002; Lee et al. 2000). The time lag is a general consequence of the upscattering of soft photons by hot electrons (Payne 1980). It is worth emphasizing that the upscattering of soft photons can take place even in situations where the electron temperature is *decreasing* as a function of time due to inverse-Compton cooling, as discussed in § 6.3. Hence the spectral softening, combined with the hard lags, strongly

imply that thermal Comptonization is playing a significant role in these sources. The hard lags are a particularly important diagnostic, since they may provide an indelible “imprint” of the time-dependent process that can be detected even when there is inadequate spectral-temporal resolution to accurately measure the sequence of spectral curves.

The time-dependent nature of the analytical solution for the Green's function obtained here provides a convenient basis for the theoretical computation of the frequency-dependent lags. By exploiting the close relationship between the Fourier and Laplace transforms, one can use the exact expression for the Laplace transformation of the energy distribution (eq. [25]) along with the Laplace transformation of the escape probability distribution to obtain the Fourier transformation of the escaping spectrum using the convolution theorem. This would yield an analytical means for computing the complex cross-spectrum and evaluating the X-ray time lags (van der Klis et al. 1987), which may represent an efficient alternative to the Monte-Carlo based simulations that are usually employed to compute the lags. The formalism developed here focuses on a homogeneous scattering cloud, and there are some indications that this may not be an appropriate model for certain galactic black-hole candidates, in which the density in the corona may vary as $1/r$ (Böttcher & Liang 1998; Kazanas, Hua, & Titarchuk 1997). However, this conclusion also depends on the shape of the cloud, and it would therefore be interesting to extract the lags using the analytical solution and compare them with the available X-ray data. Moreover, it may be possible to extend the general analytical approach taken here in order to treat inhomogeneous clouds. We plan to pursue this possibility in future work.

In addition to the continuum emission discussed above, Seyfert galaxies also appear to exhibit Fe $K\alpha$ line emission. This component of the spectrum is quite broad, and in some cases highly variable (Wang, Zhou, & Wang 1999; Wang et al. 1999; Vaughan & Edelson 2001). It is currently not clear whether the width of the line features reflects Doppler and gravitational broadening very close to the black hole (Reynolds & Wilms 2000), or perhaps broadening due to thermal Comptonization in a surrounding corona (Misra & Kembhavi 1998). Our analytical solution for the Green's function may prove to be helpful in resolving this issue since it provides an exact description of the time-dependent reprocessing of the line emission in the corona. Sample calculations illustrating the broadening of the line were presented in Figure 6, where the effects of variations in the initial energy ϵ_0 relative to the electron thermal energy kT_e were explored, along with variations in the value of the mean Compton parameter \bar{y} . The analytical expression for the time-dependent Green's function developed here is valid for arbitrary values of the initial photon energy ϵ_0 , and therefore it can be used to study the upscattering of an initial photon distribution with $\epsilon_0 \ll kT_e$, or the downscattering of initial photons with $\epsilon_0 \gg kT_e$. We reiterate that the previous analytical solution for the time-dependent Green's function derived by Payne (1980) and Zeldovich & Sunyaev (1969) is valid only for the case of very soft photons scattered by hot electrons, due to the neglect of the recoil term in the Kompaneets equation.

6.3 Thermal and dynamical effects

It has long been recognized that the injection of large quantities of soft radiation into a hot corona will almost certainly result in substantial inverse-Compton cooling of the electrons (Payne 1980; Lightman, Giacconi, & Tananbaum 1978; Guilbert, Fabian, & Ross 1982; Becker & Begelman 1986). This idea is further supported by the fact that the spectral softening observed in Seyfert X-ray transients is inconsistent with the hardening evident in the sequence of Comptonized bremsstrahlung spectra plotted in Figure 7, based on the assumption of a constant-temperature corona. We therefore conclude that the variation of the electron temperature in the corona must be included in models for the spectral evolution occurring during the flare. If the transient is very intense, the gas is expected to be radiation-dominated, and the electron temperature should therefore track the inverse-Compton temperature of the radiation (Becker & Begelman 1986; Becker 1999). This issue has been explored by Böttcher (2001), who performed Monte-Carlo simulations of disk/corona models with temperatures that responded self-consistently to the inverse-Compton cooling. They find that the inclusion of thermal effects improved the agreement between the predicted and observed X-ray time lags. If the cooling of the electrons occurs on timescales that exceed the characteristic time for the photons to diffuse out of the cloud, then the spectrum may be adequately represented using a sequence of constant-temperature (though not necessarily time-independent) models. On the other hand, if the electron temperature varies on shorter timescales, then the entire problem of thermal Comptonization must be reconsidered from first principles, including a self-consistent treatment of the temperature. It is currently unclear whether the temperature varies this rapidly during typical Seyfert transients (see discussions in Payne 1980; Petrucci et al. 2001; Nandra 2001; Malzac & Jourdain 2000). We plan to explore this question in future work.

Another issue of potential importance for models of the spectral evolution during X-ray transients is the possible dynamical response of the corona, driven by the heating and cooling of the gas. Bulk motions may be important if the gas responds hydrodynamically to the energy input, or if it is already moving, as in an accretion flow. Expansion of the corona due to heating may deplete some of the energy from the photons, and, conversely, contraction will lead to photon energization via the first-order Fermi process (“bulk Comptonization”). Although we have assumed here that the electron temperature T_e and number density n_e remain constant during the transient, in general these two quantities should be considered functions of time and position, since both will respond to the hydrodynamics and thermodynamics of the gas. Some progress has been made in understanding the effect of the bulk flow on the radiation spectrum in idealized situations. For example, Colpi (1988)

has analyzed the effect of thermal Comptonization on photons injected at an arbitrary radius into a freely-falling, spherical accretion flow using a steady-state model. She finds that the convergence of the flow can significantly alter the shape of the escaping high-energy spectrum due to a combination of photon trapping and Fermi energization. Similarly, Laurent & Titarchuk (2001) find that bulk Comptonization in quasi-spherical inflows can have a direct effect on the steady-state power-law continuum emission produced. Following a similar approach, it may be possible to incorporate the effects of bulk motion within the framework of a time-dependent model such as the one considered here.

In conclusion, we believe that the theoretical framework developed in this paper will facilitate a more complete utilization of the high-quality temporal and spectral data provided by current and future orbital X-ray observatories. The new solution for the Green's function generalizes and extends the previously known analytical solutions for thermal Comptonization, and further extensions to cases involving variable coronal temperatures and density structures may also be possible. When combined with time-resolved spectra obtained during bright X-ray flares in AGNs, these analytical solutions may allow the determination of source parameters that previously were difficult to interpret due to the necessity of running lengthy computer simulations.

The author is grateful to Demos Kazanas for several stimulating conversations, and also to the referee, Lev Titarchuk, for providing many useful comments which led to significant improvements in the manuscript.

REFERENCES

- Abramowitz, M., Stegun, I. A., 1970, *Handbook of Mathematical Functions* (NY: Dover)
- Becker, P. A., 1988, *ApJ*, 327, 772
- Becker, P. A., 1999, *Journal of Mathematical Physics*, 40, 5224
- Becker, P. A., Begelman, M. C., 1986, *ApJ*, 310, 534
- Böttcher, M., 2001, *ApJ*, 553, 960
- Böttcher, M., Liang, E. P., 1998, *ApJ*, 506, 281
- Butkov, E., 1968, *Mathematical Physics* (London: Addison-Wesley)
- Chapline, G., Jr., Stevens, J., 1973, *ApJ*, 184, 1041
- Colafrancesco, S. et al., 1997, *ApJ*, 479, 1
- Colpi, M., 1988, *ApJ*, 326, 223
- Ghisellini, G., Celotti A., 1999, *ApJ*, 511, L93
- Gradshteyn, I. S., Ryzhik, I. M., 1980, *Table of Integrals, Series, and Products* (Academic Press: London)
- Guilbert, P. W., Fabian, A. C., Ross, R. R., 1982, *MNRAS*, 199, 763
- Illarionov, A. F., Sunyaev, R. A., 1975a, *Sov. Astron.*, 18, 413
- Illarionov, A. F., Sunyaev, R. A., 1975b, *Sov. Astron.*, 18, 691
- Iwasawa, K. et al., 2000, *MNRAS*, 318, 879
- Kazanas, D., Hua, X.-M., Titarchuk, L., 1997, *ApJ*, 480, 735
- Katz, J. I., 1976, *ApJ*, 206, 910
- Kitamoto, S., 1989, in *Proc. 23rd ESLAB Symposium*, p. 231
- Kompaneets, A. S., 1957, *Sov. Phys.-JETP*, 4, 730
- König, M. et al., 1997, *A&A*, 322, 747
- Lacombe, C., 1977, *A&A*, 54, 1
- Lapidus, I. I., Sunyaev, R. A., Titarchuk, L. G., 1987, *Sov. Astron. Lett.*, 12, 383
- Laurent, P., Titarchuk, L. G., 2001, *ApJ*, 562, L67
- Lawrence, A., 1980, *MNRAS*, 192, 83
- Lee, J. C. et al., 2000, *MNRAS*, 318, 857
- Liang, E. P. et al., 1999, *ApJ*, 519, L21
- Lightman, A. P., Giacconi, R., Tananbaum, H., 1978, *ApJ*, 224, 375
- Lyubarskii, Y. E., Sunyaev, R. A., 1982, *Sov. Astron. Lett.*, 8, 330
- Malzac, J., Jourdain, E., 2000, *A&A*, 359, 843
- Mereghetti, S., 1993, *A&A*, 97, 249
- Merloni, A., Fabian, A. C., 2001, *MNRAS*, 328, 958
- Miller, J. A., Ramaty, R., 1989, *ApJ*, 344, 973
- Misra, R., Kembhavi, A. K., 1998, *ApJ*, 499, 205
- Mittaz, J. P. D., Branduardi-Raymont, G., 1989, *MNRAS*, 238, 1029
- Miyamoto, S. M. et al., 1991, *ApJ*, 383, 784
- Nandra, K., 2001, *Advances in Space Research*, 28, 295
- Park, B. T., Petrosian, V., Schwartz, R. A., 1997, *ApJ*, 489, 358

- Payne, D. G., 1980, ApJ, 237, 951
 Payne, D. G., Blandford, R. D., 1981, MNRAS, 196, 781
 Petrucci, P. O. et al., 2001, MNRAS, 328, 501
 Reynolds, C. S., Wilms, J., 2000, ApJ, 533, 821
 Reynolds, C. S. et al., 1999, ApJ, 514, 164
 Ross, R. R., Fabian, A. C., Young, A. J., 1999, MNRAS, 306, 461
 Rybicki, G. B., Lightman, A. P., 1979, Radiative Processes in Astrophysics (NY: Wiley)
 Schlickeiser, R., 1984, A&A, 136, 227
 Schlickeiser, R., Sievers, A., Thiemann, H., 1987, A&A, 182, 21
 Shapiro, S. L., Lightman, A. P., Eardley, D. M., 1976, ApJ, 204, 187
 Shimon, M., Rephaeli, Y., 2002, ApJ, 575, 12
 Slater, L. J., 1960, Confluent Hypergeometric Functions (Cambridge Univ. Press, Cambridge, England)
 Smith, D. M., Heindl, W. A., Swank, J. H., 2002, ApJ, 569, 362
 Stollman, G. M. et al., 1987, MNRAS, 227, 7
 Sunyaev, R. A., Titarchuk, L. G., 1980, A&A, 86, 121
 Sunyaev, R. A., Zeldovich, Ya. B., 1970, Ap&SS, 7, 20
 Tanaka, Y., 1989, in Proc. 23rd ESLAB Symposium, p. 3
 Tananbaum, H. et al., 1978, ApJ, 223, 74
 Titarchuk, L. G., 1988, Sov. Astron. Lett., 14, 229
 Titarchuk, L., Lyubarskij, Y., 1995, ApJ, 450, 876
 Titarchuk, L., Mastichiadis, A., Kylafis, N. D., 1997, ApJ, 487, 834
 Titarchuk, L. G., Shrader, C. R., 2002, ApJ, 567, 1057
 Titarchuk, L., Zannias, T., 1998, ApJ, 493, 863
 Ulrich, M.-H., 2000, Astron. Ap. Rev., 10, 135
 van der Klis, M. et al., 1987, ApJ, 319, L13
 Vaughan, S., Edelson, R., 2001, ApJ, 548, 694
 Wang, J.-X., Zhou, Y.-Y., Wang, T.-G., 1999, ApJ, 523, L129
 Wang, J.-X. et al., 1999, ApJ, 516, L65
 Zeldovich, Ya. B., Sunyaev, R. A., 1969, Ap&SS, 4, 301
 Zdziarski, A. A. et al., 2002, ApJ, 578, 357

APPENDIX A: MATHEMATICAL DETAILS

A1 Formal solution for the Laplace transform

The Laplace transform

$$L(x, x_0, s) \equiv \int_0^\infty e^{-sy} f_G(x, x_0, y) dy \quad (\text{A1})$$

of the Green's function distribution $f_G(x, x_0, y)$ satisfies the inhomogeneous ordinary differential equation

$$\frac{1}{x^2} \frac{d}{dx} \left[x^4 \left(L + \frac{dL}{dx} \right) \right] - sL = -x_0^{-2} \delta(x - x_0). \quad (\text{A2})$$

The homogeneous equation obtained when $x \neq x_0$ has the solutions

$$L(x, x_0, s) = \begin{cases} A x^{-2} e^{-x/2} M_{2, \mu}(x), & x \leq x_0, \\ B x^{-2} e^{-x/2} W_{2, \mu}(x), & x \geq x_0, \end{cases} \quad (\text{A3})$$

where $M_{2, \mu}(x)$ and $W_{2, \mu}(x)$ denote Whittaker's functions, and

$$\mu(s) \equiv \left(\frac{9}{4} + s \right)^{1/2}. \quad (\text{A4})$$

Asymptotic analysis indicates that these are the only functions that yield convergent results for the photon number and energy densities. The constants A and B appearing in equation (A3) are determined by imposing continuity and derivative jump conditions on the transform L . The solution for L must be continuous at $x = x_0$ in order to avoid an infinite flux of photons in the energy space. The continuity condition requires

$$A M_{2, \mu}(x_0) = B W_{2, \mu}(x_0). \quad (\text{A5})$$

Furthermore, the derivative dL/dx must display a jump at $x = x_0$ given by

$$\lim_{\varepsilon \rightarrow 0} \left. \frac{dL}{dx} \right|_{x_0+\varepsilon} - \left. \frac{dL}{dx} \right|_{x_0-\varepsilon} = -\frac{1}{x_0^4}, \quad (\text{A6})$$

which is obtained by integrating equation (A1) in a narrow range around $x = x_0$.

Utilization of the continuity and derivative jump conditions yields for A and B the solutions

$$A = \frac{-e^{x_0/2} x_0^{-2} W_{2,\mu}(x_0)}{w(x_0)}, \quad B = \frac{-e^{x_0/2} x_0^{-2} M_{2,\mu}(x_0)}{w(x_0)}, \quad (\text{A7})$$

where the Wronskian of the two solutions is defined by

$$w(x) \equiv M_{2,\mu}(x) \frac{d}{dx} W_{2,\mu}(x) - W_{2,\mu}(x) \frac{d}{dx} M_{2,\mu}(x). \quad (\text{A8})$$

The Wronskian can be evaluated using equations (13.1.22), (13.1.32), and (13.1.33) of Abramowitz & Stegun (1970), which yields

$$w(x) = -\frac{\Gamma(1+2\mu)}{\Gamma(\mu-3/2)}. \quad (\text{A9})$$

Combining results, we find that the formal solution for the Laplace transform is given by

$$L(x, x_0, s) = \frac{\Gamma(\mu-3/2)}{\Gamma(1+2\mu)} x_0^{-2} x^{-2} e^{(x_0-x)/2} \begin{cases} W_{2,\mu}(x_0) M_{2,\mu}(x), & x \leq x_0, \\ M_{2,\mu}(x_0) W_{2,\mu}(x), & x \geq x_0, \end{cases} \quad (\text{A10})$$

or, equivalently,

$$L(x, x_0, s) = \frac{\Gamma(\mu-3/2)}{\Gamma(1+2\mu)} x_0^{-2} x^{-2} e^{(x_0-x)/2} M_{2,\mu}(x_{\min}) W_{2,\mu}(x_{\max}), \quad (\text{A11})$$

where

$$x_{\min} \equiv \min(x, x_0), \quad x_{\max} \equiv \max(x, x_0). \quad (\text{A12})$$

The solution for the Laplace transform $L(x, x_0, s)$ is closely related to the Green's function for the steady-state problem developed by Sunyaev & Titarchuk (1980), as discussed in § 5.4. Simple poles are located where the function $\Gamma(\mu-3/2)$ diverges, which occurs when the quantity $\mu-3/2$ is zero or a negative integer. The evaluation of the residues at the simple poles is carried out in the next section, and the inverse Laplace transformation is discussed in § 3.2.

A2 Evaluation of the residues

We found in § 3 that the Green's function energy distribution can be expressed as

$$f_G(x, x_0, y) = -\frac{1}{2\pi i} \int_N^O e^{sy} L(x, x_0, s) ds - \frac{1}{2\pi i} \int_P^Q e^{sy} L(x, x_0, s) ds + \sum_{n=1}^2 \text{Res}(s_n), \quad (\text{A13})$$

in the limit $r_1 \rightarrow \infty$, $r_2 \rightarrow 0$ (see Fig. 1), where the transform $L(x, x_0, s)$ is given by equation (A10) and $\text{Res}(s_n)$ is the residue associated with the pole at $s = s_n$. In our problem, simple poles are located at $s_1 = 0$ and $s_2 = -2$, and the corresponding residues are computed using the formulas (Butkov 1968)

$$\text{Res}(s_1) = \lim_{s \rightarrow 0} s L(x, x_0, s) e^{sy}, \quad \text{Res}(s_2) = \lim_{s \rightarrow -2} (s+2) L(x, x_0, s) e^{sy}. \quad (\text{A14})$$

Because the poles correspond to the singularities of the function $\Gamma(\mu-3/2)$, evaluation of the residues requires utilization of the asymptotic results

$$\lim_{s \rightarrow 0} s \Gamma(\mu-3/2) = 3, \quad \lim_{s \rightarrow -2} (s+2) \Gamma(\mu-3/2) = -1, \quad (\text{A15})$$

which follow from the definition of $\mu(s)$ given by equation (A4). We can show that the functions $M_{2,\mu}(x)$ and $W_{2,\mu}(x)$ reduce to combinations of Laguerre polynomials and exponentials at the points $s = 0$ and $s = -2$. In particular, using equations (13.1.2), (13.1.3), (13.1.32), and (13.1.33) from Abramowitz & Stegun (1970), we obtain for $s = 0$ the results

$$M_{2,\mu}(x) \Big|_{s=0} = e^{-x/2} x^2, \quad W_{2,\mu}(x) \Big|_{s=0} = e^{-x/2} x^2. \quad (\text{A16})$$

Likewise, for $s = -2$ we find that

$$M_{2,\mu}(x) \Big|_{s=-2} = e^{-x/2} x \left(1 - \frac{x}{2}\right), \quad W_{2,\mu}(x) \Big|_{s=-2} = -e^{-x/2} x (2-x). \quad (\text{A17})$$

Combining equation (A10) with equations (A14) - (A17), we establish that the residues are given by

$$\text{Res}(s_1) = \frac{1}{2} e^{-x}, \quad \text{Res}(s_2) = \frac{1}{2} e^{-x-2y} (2-x)(2-x_0) x^{-1} x_0^{-1}. \quad (\text{A18})$$

A3 Integration along the branch cut

The remaining integrations in equation (A13) along the upper and lower segments NO and PQ , respectively, need to be handled carefully because of the presence of the branch cut extending from $s = -9/4$ to $s = -\infty$ (see Fig. 1) in the definition of $\mu(s)$ (eq. [A4]). We proceed by transforming to a new variable of integration, u , defined by

$$u^2 \equiv -\frac{9}{4} - s, \quad (\text{A19})$$

with $u = 0$ at the branch point. This is useful because the integration bounds in equation (A13) now transform to the convenient values $(0, \infty)$. In terms of u , equation (A4) for $\mu(s)$ can be rewritten along the upper and lower segments as

$$\mu(u) = iu, \quad \text{segment } NO, \quad (\text{A20})$$

$$\mu(u) = -iu, \quad \text{segment } PQ. \quad (\text{A21})$$

The sign change between the two expressions for $\mu(u)$ along the two segments reflect the two different branches of the complex square root function. Using equation (A11) to substitute for $L(x, x_0, s)$ in equation (A13) and transforming the variable of integration from s to u , with $ds = -2u du$, we obtain

$$f_G(x, x_0, y) = \frac{e^{-9y/4} e^{(x_0-x)/2}}{\pi i x_0^2 x^2} \int_0^\infty e^{-u^2 y} \left[\frac{\Gamma(-3/2 - iu)}{\Gamma(1 - 2iu)} M_{2, -iu}(x_{\min}) W_{2, -iu}(x_{\max}) \right. \\ \left. - \frac{\Gamma(-3/2 + iu)}{\Gamma(1 + 2iu)} M_{2, iu}(x_{\min}) W_{2, iu}(x_{\max}) \right] u du + \sum_{n=1}^2 \text{Res}(s_n), \quad (\text{A22})$$

where the residues are given by equations (A18). From the definition of the $W_{2, \mu}(x)$ function,

$$W_{2, \mu}(x) \equiv \frac{\Gamma(-2\mu)}{\Gamma(-\mu - 3/2)} M_{2, \mu}(x) + \frac{\Gamma(2\mu)}{\Gamma(\mu - 3/2)} M_{2, -\mu}(x), \quad (\text{A23})$$

it follows that

$$W_{2, iu}(x) = W_{2, -iu}(x), \quad (\text{A24})$$

and therefore we can rewrite our expression for the Green's function as

$$f_G(x, x_0, y) = \frac{e^{-9y/4} e^{(x_0-x)/2}}{\pi i x_0^2 x^2} \int_0^\infty e^{-u^2 y} W_{2, iu}(x_{\max}) \left[\frac{\Gamma(-3/2 - iu)}{\Gamma(1 - 2iu)} M_{2, -iu}(x_{\min}) \right. \\ \left. - \frac{\Gamma(-3/2 + iu)}{\Gamma(1 + 2iu)} M_{2, iu}(x_{\min}) \right] u du + \sum_{n=1}^2 \text{Res}(s_n). \quad (\text{A25})$$

Based on equation (A23), we can show that the factor in square brackets in equation (A25) is given by

$$\left[\frac{\Gamma(-3/2 - iu)}{\Gamma(1 - 2iu)} M_{2, -iu}(x_{\min}) - \frac{\Gamma(-3/2 + iu)}{\Gamma(1 + 2iu)} M_{2, iu}(x_{\min}) \right] = \frac{\Gamma(-3/2 - iu) \Gamma(-3/2 + iu)}{\Gamma(2iu) \Gamma(1 - 2iu)} W_{2, iu}(x_{\min}). \quad (\text{A26})$$

The products of gamma functions on the right-hand side of this expression can be simplified using the identities

$$\Gamma(2iu) \Gamma(1 - 2iu) = \frac{\pi}{2i \sinh(\pi u) \cosh(\pi u)}, \quad (\text{A27})$$

$$\Gamma(-3/2 - iu) \Gamma(-3/2 + iu) = \frac{16\pi}{\cosh(\pi u) (1 + 4u^2) (9 + 4u^2)}. \quad (\text{A28})$$

Combining equations (A18), (A25), (A26), (A27), and (A28), we obtain after some algebra

$$f_G(x, x_0, y) = \frac{32}{\pi} e^{-9y/4} x_0^{-2} x^{-2} e^{(x_0-x)/2} \int_0^\infty e^{-u^2 y} \frac{u \sinh(\pi u)}{(1 + 4u^2)(9 + 4u^2)} \\ \times W_{2, iu}(x_0) W_{2, iu}(x) du + \frac{e^{-x}}{2} + \frac{e^{-x-2y}}{2} \frac{(2-x)(2-x_0)}{x_0 x}. \quad (\text{A29})$$

This is our final result for the Green's function, which appears as equation (33) in the main text. Series expansions for the Whittaker functions are provided in § A.4. A self-contained FORTRAN program that evaluates the Whittaker functions and performs the integration in equation (A29) to yield the Green's function is available from the author upon request. We point

out that a related integral involving a single Whittaker function was worked out by Kompaneets (1957) in collaboration with I. M. Gelfand in order to describe the variation of the mean photon energy due to thermal Comptonization, as discussed in § 4.2 (see eq. [46]).

A4 Series expansions for the Whittaker functions

In order to carry out the integration in the analytical solution for the Green's function given by equations (33) and (A29), we need to be able to evaluate the Whittaker function $W_{2,iu}(x)$ for both large and small values of the argument x . Furthermore, the solution we have obtained for the optically thin bremsstrahlung initial spectrum (eq. [67]) requires the evaluation of the functions $W_{1,iu}(x_*)$, $W_{0,iu}(x_*)$, $W_{-1,iu}(x_*)$, and $W_{-2,iu}(x_*)$ for small values of the low-energy cutoff x_* (see eq. [63]). We shall develop the necessary expansions below.

A4.1 Expansion for Small x

Based on the definition of $W_{\kappa,\mu}(x)$ given by equation (13.1.34) of Abramowitz & Stegun (1970), we can write

$$W_{\kappa,iu}(x) \equiv \frac{\Gamma(-2iu)}{\Gamma(1/2 - \kappa - iu)} M_{\kappa,iu}(x) + \frac{\Gamma(2iu)}{\Gamma(1/2 - \kappa + iu)} M_{\kappa,-iu}(x). \quad (\text{A30})$$

The two terms on the right-hand side are complex conjugates of each other, and therefore $W_{\kappa,iu}(x)$ is purely real. Hence we obtain

$$W_{\kappa,iu}(x) = 2 \operatorname{Re} \left\{ \frac{\Gamma(-2iu)}{\Gamma(1/2 - \kappa - iu)} M_{\kappa,iu}(x) \right\}. \quad (\text{A31})$$

For small values of x , the function $M_{\kappa,\mu}(x)$ can be evaluated using the series

$$M_{\kappa,iu}(x) = e^{-x/2} x^{iu+1/2} \sum_{n=0}^{\infty} \frac{(1/2 - \kappa + iu)_n}{(1 + 2iu)_n} \frac{x^n}{n!}, \quad (\text{A32})$$

where $(a)_n$ denotes the Pochhammer symbol, defined by (Abramowitz & Stegun 1970)

$$(a)_n \equiv \begin{cases} 1, & n = 0, \\ a(a+1) \cdots (a+n-1), & n \geq 1. \end{cases} \quad (\text{A33})$$

Combining expressions, we obtain finally

$$W_{\kappa,iu}(x) = 2 e^{-x/2} x^{1/2} \sum_{n=0}^{\infty} \frac{x^n}{n!} \operatorname{Re} \left\{ \frac{\Gamma(-2iu) x^{iu}}{\Gamma(1/2 - \kappa - iu)} \frac{(1/2 - \kappa + iu)_n}{(1 + 2iu)_n} \right\}. \quad (\text{A34})$$

This expansion can be used to evaluate each of the Whittaker functions $W_{1,iu}(x_*)$, $W_{0,iu}(x_*)$, $W_{-1,iu}(x_*)$, and $W_{-2,iu}(x_*)$ appearing in equation (67).

An application of special interest is the function $W_{2,iu}(x)$ appearing in equation (33) for the Green's function. We obtain in this case

$$W_{2,iu}(x) = 2 e^{-x/2} x^{1/2} \sum_{n=0}^{\infty} \frac{x^n}{n!} \operatorname{Re} \left\{ \frac{\Gamma(-2iu) x^{iu}}{\Gamma(-3/2 - iu)} \frac{(-3/2 + iu)_n}{(1 + 2iu)_n} \right\}. \quad (\text{A35})$$

In practice, we use this expansion to evaluate $W_{2,iu}(x)$ for $x \leq x_{\text{mid}}(u)$, where

$$x_{\text{mid}}(u) \equiv \begin{cases} 20, & u \leq 10/3, \\ 10 + 3u, & u \geq 10/3. \end{cases} \quad (\text{A36})$$

We emphasize that the functions $W_{\kappa,iu}(x)$ and $W_{2,iu}(x)$ are purely real, despite the appearance of the imaginary number i in equations (A34) and (A35). The complex gamma function $\Gamma(z)$ can be evaluated using equation (6.1.48) from Abramowitz & Stegun (1970).

A4.2 Expansion for Large x

The Whittaker functions $W_{1,iu}(x_*)$, $W_{0,iu}(x_*)$, $W_{-1,iu}(x_*)$, and $W_{-2,iu}(x_*)$ appearing in equation (67) for the bremsstrahlung particular solution need only be evaluated for small values of the low-energy cutoff x_* , and therefore equation (A34) is sufficient for this case. However, the function $W_{2,iu}(x)$ appearing in equation (33) for the Green's function must be evaluated for general, positive values of x . We can use equation (A35) to compute $W_{2,iu}(x)$ when $x \leq x_{\text{mid}}(u)$. For larger values of x , a convergent series for $W_{2,iu}(x)$ can be obtained by combining equations (13.1.33) and (13.5.2) of Abramowitz & Stegun (1970), which yields

$$W_{2,iu}(x) = e^{-x/2} x^2 \sum_{n=0}^{\infty} \frac{(-3/2 + iu)_n (-3/2 - iu)_n}{n! (-x)^n}. \quad (\text{A37})$$

The Pochhammer symbols in this equation are complex conjugates of each other, and therefore our result for $W_{2,iu}(x)$ can be rewritten as the completely real expression

$$W_{2,iu}(x) = e^{-x/2} x^2 \left\{ 1 + \sum_{n=1}^{\infty} \frac{(-x)^{-n}}{n!} \prod_{m=1}^n \left[\left(\frac{5}{2} - m \right)^2 + u^2 \right] \right\}. \quad (\text{A38})$$

We use this formula to evaluate $W_{2,iu}(x)$ when $x > x_{\text{mid}}(u)$, where $x_{\text{mid}}(u)$ is defined by equation (A36). In performing the numerical integration in equation (33), it is sufficient to treat the domain $0 \leq u \leq 20$ because larger values of u make a negligible contribution to the integral.

This paper has been typeset from a $\text{T}_{\text{E}}\text{X}/\text{L}^{\text{A}}\text{T}_{\text{E}}\text{X}$ file prepared by the author.